

PL-TR-96-2078

**ANALYSIS OF IONOSPHERIC PARAMETERS BASED  
ON DMSP SSIES DATA USING THE *DBASE4* AND  
*NADIA* PROGRAMS**

Marc R. Hairston  
Roderick A. Heelis

University of Texas at Dallas  
William B. Hanson Center for Space Sciences  
PO Box 830688 MS FO22  
Richardson, TX 75083-0688

4 April 1996

Final Report  
1 March 1993 – 31 March 1996

Approved for public release; distribution unlimited

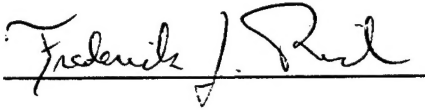


**PHILLIPS LABORATORY  
Directorate of Geophysics  
AIR FORCE MATERIEL COMMAND  
HANSCOM AIR FORCE BASE, MA 01731-3010**

19960909 014

DATE QUALIFIED FOR RELEASE 1

"This Technical report has been reviewed and is approved for publication"



FREDERICK RICH  
Contract Manager



EDWARD G. MULLEN  
Branch Chief



RITA C. SAGALYN  
Division Director

This report has been reviewed by the ESC Public Affairs Office (PA) and is releasable to the National Technical Information Service (NTIS).

Qualified requestors may obtain additional copies from the Defense Technical Information Center (DTIC). All others should apply to the National Technical Information Service (NTIS).

If your address has changed, or if you wish to be removed from the mailing list, or if the addressee is no longer employed by your organization, please notify PL/IM, 29 Randolph Road, Hanscom AFB, MA 01731-3010. This will assist us in maintaining a current mailing list.

Do not return copies of this report unless contractual obligations or notices on a specific document requires that it be returned.

REPORT DOCUMENTATION PAGE			Form Approved OMB No. 0704-0188	
<small>Public reporting burden for this collection of information is estimated to average 1 hour per response, including the time for reviewing instructions, searching existing data sources, gathering and maintaining the data needed, and completing and reviewing the collection of information. Send comments regarding this burden estimate or any other aspect of this collection of information, including suggestions for reducing this burden, to Washington Headquarters Services, Directorate for Information Operations and Reports, 1215 Jefferson Davis Highway, Suite 1204, Arlington, VA 22202-4302, and to the Office of Management and Budget, Paperwork Reduction Project (0704-0188), Washington, DC 20503.</small>				
1. AGENCY USE ONLY (Leave blank)	2. REPORT DATE 4 April 1996	3. REPORT TYPE AND DATES COVERED Final (1 March 1993--31 March 96)		
4. TITLE AND SUBTITLE Analysis of Ionospheric Parameters Based on DMSP SSIES Data Using the DBASE4 and NADIA Programs		5. FUNDING NUMBERS Contract F19628-93-K-0007 PE 35160F PR 2311 TAGB WUMA		
6. AUTHOR(S) Marc R. Hairston Roderick A. Heelis				
7. PERFORMING ORGANIZATION NAME(S) AND ADDRESS(ES) William B. Hanson Center for Space Sciences University of Texas at Dallas PO Box 830688 F022 Richardson, TX 75083-0688		8. PERFORMING ORGANIZATION REPORT NUMBER		
9. SPONSORING/MONITORING AGENCY NAME(S) AND ADDRESS(ES) Phillips Laboratory 29 Randolph Road Hanscom AFB, MA 01731-3010 Contract manager: Frederick Rich/GPSP		10. SPONSORING/MONITORING AGENCY REPORT NUMBER  PL-TR-96-2078		
11. SUPPLEMENTARY NOTES				
12a. DISTRIBUTION/AVAILABILITY STATEMENT  Approved for public release; distribution unlimited		12b. DISTRIBUTION CODE		
13. ABSTRACT (Maximum 200 words)  This report covers further upgrades and extentions of the previously submitted DBASE4 analysis program which uses DMSP/SSIES data to derive an electrostatic potential distribution in the polar ionosphere and attempt to match it to one of the three standard Heppner-Maynard distribution patterns. These results form part of the input for the operational Magnetospheric Specification Model being run by 50th Air Weather. This report uses archived data to evaluate the performance of the existing code and documents the changes which were made to improve it. It also uses archived interplanetary magnetic field data (IMF) to compare the identified pattern with the actual IMF orientation in order to evaluate the quality of the output based only on the three Heppner-Maynard models. As the solar cycle reached its minimum in 1995-1996, the changes in the ionospheric densities and compositions were reflected by changes in quality of the data from the SSIES instrument. A major revision in the analysis algorithms was written and tested to insure that a majority of the polar passes could still be used for the MSM analysis. This revised version of DBASE4 is called Nominal / Anomalous (passes) Database for Ionospheric Analysis (NADIA) and its design and performance are described in this report.				
14. SUBJECT TERMS DMSP; ionosphere; ionospheric plasma; ionospheric convection; solar cycle; spacecraft data analysis			15. NUMBER OF PAGES 54	
			16. PRICE CODE	
17. SECURITY CLASSIFICATION OF REPORT unclassified	18. SECURITY CLASSIFICATION OF THIS PAGE unclassified	19. SECURITY CLASSIFICATION OF ABSTRACT unclassified	20. LIMITATION OF ABSTRACT SAR	

## Table of Contents

1. Introduction.....	1
2. Review of the DBASE4 operations and algorithms.....	1
3. Building the DBASE4 database.....	10
4. Revisions of the output of DBASE4 to suit MSM operations.....	12
5. Comparison of Heppner–Maynard model selection results with actual IMF data.....	19
6. Revision of the origin locator algorithm in DBASE4.....	29
7. Introduction to NADIA.....	33
NADIA part 1: Dealing with data gaps.....	34
NADIA part 2: Dealing with light ion plasma and “fuzzy” endpoints.....	38
8. Conclusion.....	45
9. Recommendation for Future Work.....	46
Appendix: Scientific Papers Published and Professional Talks Given During this Contract.....	48
References.....	50

## **1. Introduction**

At the end of 1992, the Center for Space Sciences at the University of Texas at Dallas delivered to the Air Force, through Phillips Laboratory, a research-grade computer program entitled DMSPDBASE4 (hereafter referred to simply as DBASE4). This program processed the telemetry from the DMSP SSIES drift meter instrument and calculated the electrostatic potential drop across the polar ionosphere, then attempted to classify the overall convection flow pattern based on this one crossing signature. This code was adapted by Air Weather Service for use as an operational program providing input to the Magnetospheric Specification Model (MSM) operational code. During the past three years, we have continued to modify and upgrade this code in order to provide more reliable results as both the conditions in the ionosphere changed, as well as our understanding of the ionosphere and the data analysis routines grew. This final report details the work performed during this time.

The major work falls into three categories: building a database using DBASE4 to use for testing new versions of models and analysis procedures, dealing with requests from 50th Air Weather, Phillips Laboratories, and Rice University (the authors of the MSM code) to provide "fixes" to the DBASE4 code, and writing a final upgrade of the code to compensate for the reduced performance of the drift meter during the time of the solar minimum. This new upgrade is being delivered to Phillips Laboratory along with this report and has been renamed NADIA, which stands for Nominal / Anomalous (passes) Database for Ionospheric Analysis.

## **2. Review of the DBASE4 Operations and Algorithms**

The full description of the operations and reasoning behind the algorithms used in DBASE4 can be found in the previous report (*Hairston and Heelis, 1993*), and the earlier

report about its predecessor DMSPPOTMOD (*Heelis and Hairston, 1990*). Rather than repeat all the detailed information, this section will give only an outline of the program. Readers interested in a more complete explanation are referred to the earlier reports. Also, we will refer to sections of that program as "Block X"; one should refer to the earlier reports for further explanation of these sections.

As the solar wind and the associated interplanetary magnetic field (IMF) flow past the Earth's magnetosphere, they act as a generator to produce an electrostatic potential drop across the magnetopause. This potential drop drives many of the processes which occur in the magnetosphere and ionosphere. Since the orientation of the IMF (which affects the strength of the coupling between the IMF and the magnetosphere) is constantly changing, then this input to the magnetosphere is highly variable. Attempting to measure this potential drop across the large region of the magnetopause (generally about 30 Earth radii in diameter) would be a major undertaking. However, this potential drop conveniently maps from the magnetopause down to the much smaller region of the polar ionosphere. Thus, a single satellite crossing the polar cap region "sees" the potential distribution across the magnetosphere in about 15 to 20 minutes. This information can be used as inputs into models of the magnetosphere such as the MSM.

The overall shape of this potential distribution across the high-latitude ionosphere varies with conditions in the IMF. When the IMF is steady for some time and oriented strongly northward ( $B_z$  positive), then there is little coupling between the IMF and the Earth's magnetosphere. As a result, the overall potential drop is relatively low (less than 40 kV) and the ion circulation pattern in the ionosphere (which follows the lines of electric equipotentials) is disorganized and composed of multiple circulation cells. However, when the IMF is steady for tens of minutes and pointed southward ( $B_z$  negative) or weakly northward, then the IMF is more strongly coupled to the magnetosphere and the high-latitude poten-

tial drop is larger. The size of the potential drop increases as the magnitude of the southward IMF component increases. Generally, the observed drops during these periods are in the 60 to 100 kV range, although drops as high as 260 kV have been observed during magnetic substorm periods. During these periods, the ion flow circulation pattern in both polar ionospheres is organized into two large cells: a counter-clockwise rotating (if seen looking from above the north pole) cell on the dawn side which corresponds to the positive potential region, and a clockwise rotating (if seen looking from above the north pole) cell on the dusk side which corresponds to the negative potential region. The size of these two cells and the location of the zero potential line, which is the boundary between them, is a function of the  $B_y$  orientation of the IMF. Figure 1 shows the three Heppner-Maynard patterns for the ion flow/potential distribution patterns in the ionosphere for three different IMF orientations (*Heppner and Maynard, 1987*).

Starting with the DMSP F8 launch in June 1987, all of the DMSP satellites have carried the Special Sensor-Ion, Electrons, Scintillation (SSIIES) instrument package to provide data about the plasma environment in the ionosphere at the DMSP altitude of roughly 800 kilometers. All of the DMSP spacecraft are in polar orbits which precess at such a rate that the orbit stays in about the same local time plane throughout the year. As the spacecraft flies through the polar ionospheric regions, the drift meter measures the horizontal and vertical ion flows at right angles to the spacecraft's trajectory. Combining these flow data with the Earth's magnetic field vectors derived from a computer model provides the electric field along the satellite's trajectory. Integrating these field data across the polar cap gives an electrostatic potential curve along the spacecraft's path (Figure 2). From this curve, we can obtain a measurement of the total observed potential drop (from the maximum to the minimum), and from the position of the zero point relative to the locations of the maximum and minimum, we can categorize the overall shape of the potential distribution.

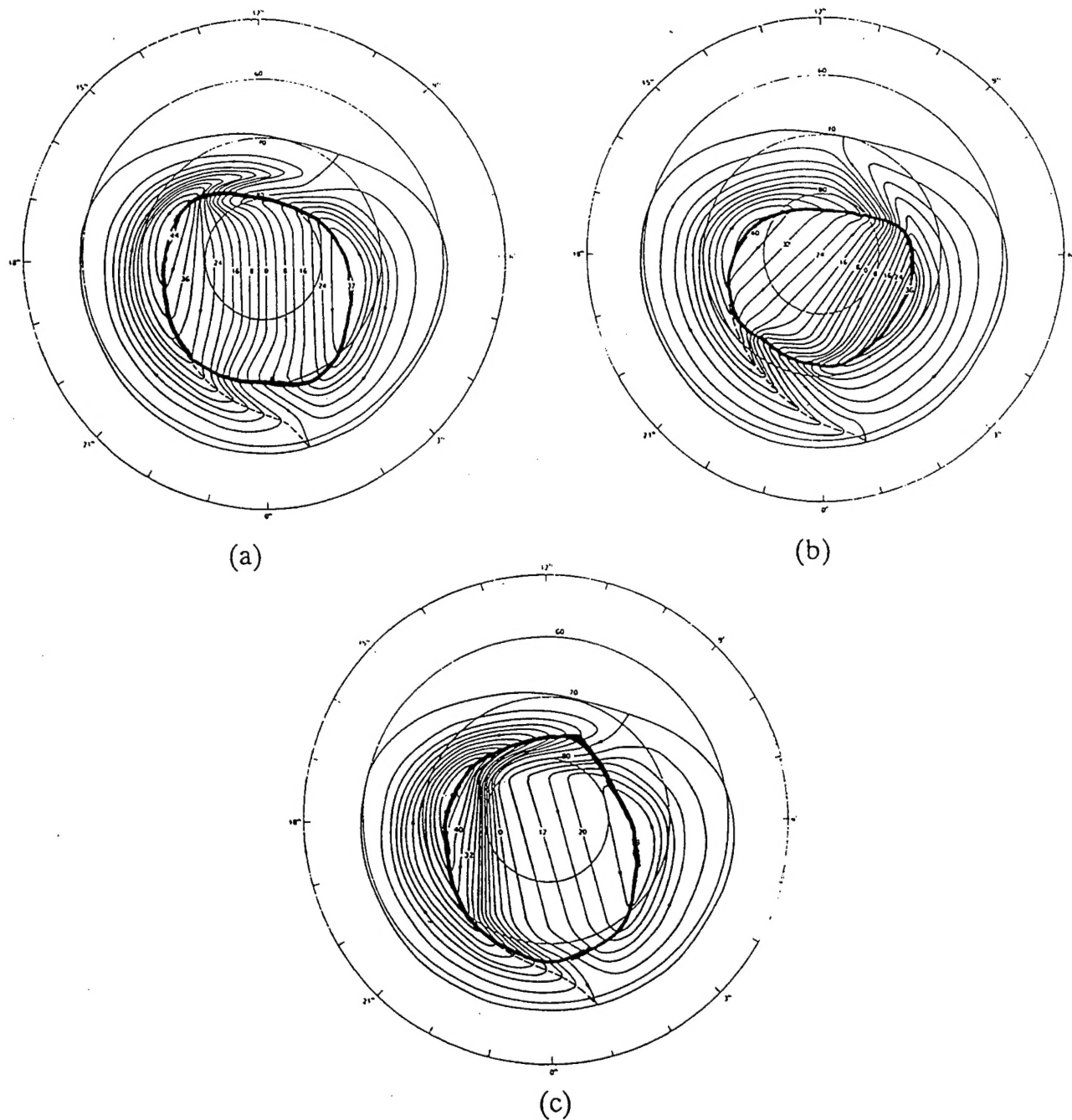


Figure 1. These are the three Heppner – Maynard patterns for the electrostatic potential distribution in the polar ionosphere (Heppner and Maynard, 1987). This figure shows pattern A / model number 2 (a), pattern BC / model number 1 (b), and pattern DE / model number 3 (c). The convection reversal boundary has been highlighted on all three patterns. Note that because of the Harang discontinuity on the nightside, there is some ambiguity as to the exact location of the boundary in the region between 2100 to 0100 magnetic local time.

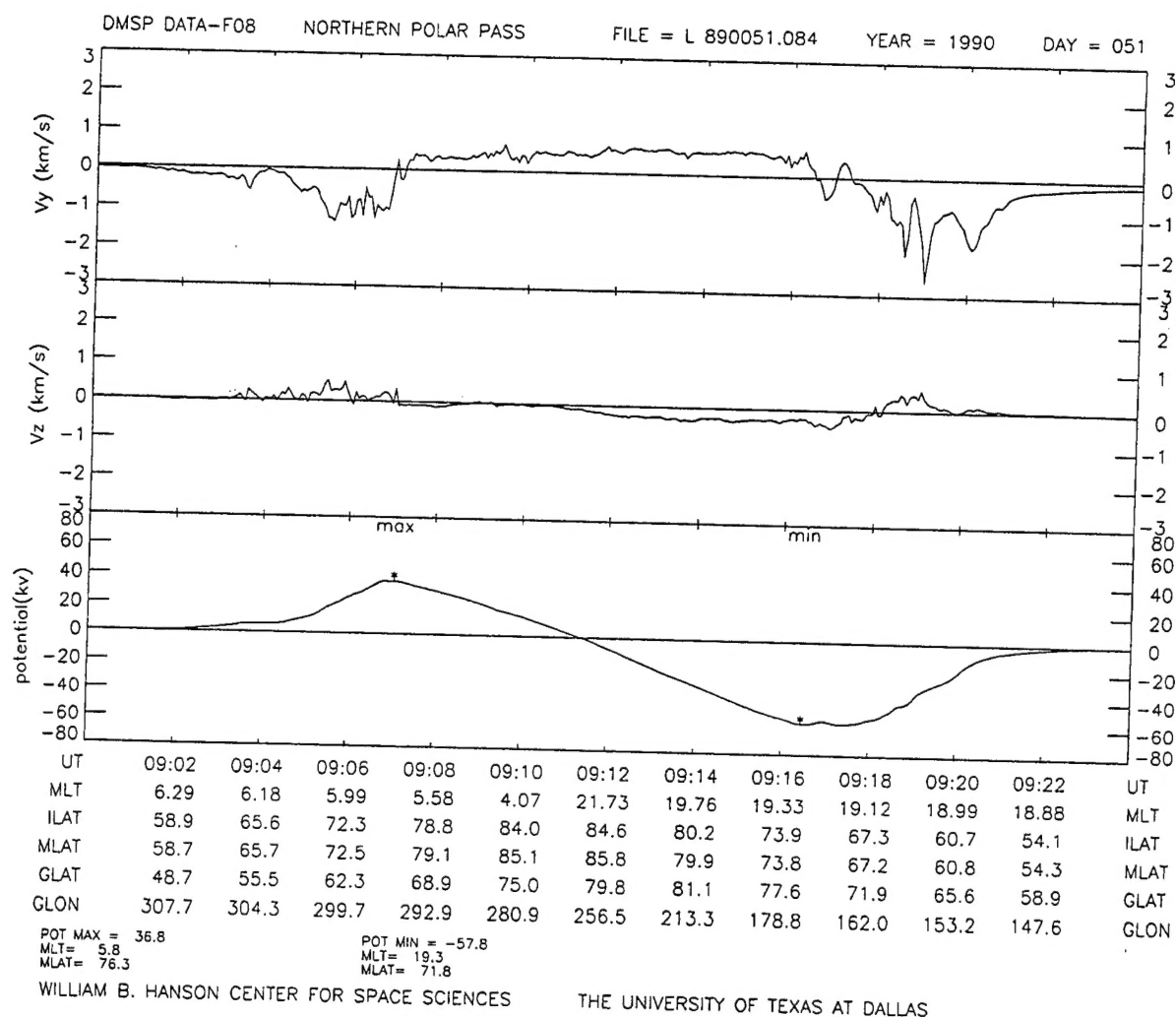
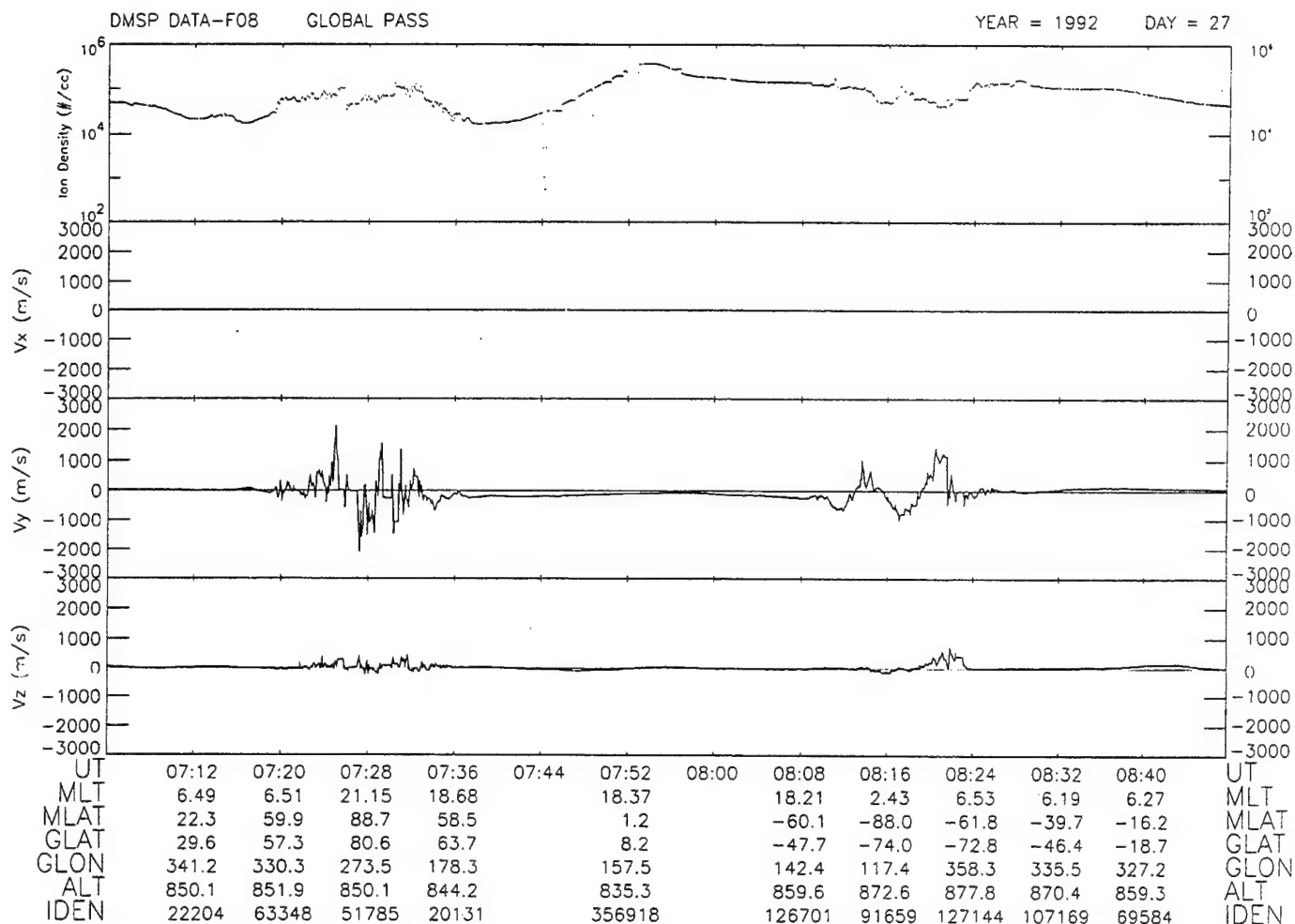


Figure 2. This is a data plot from a typical polar pass. This is a northern polar pass by F8 so the spacecraft goes from the dawnside to the duskside in this plot. The top panel shows the horizontal ion flow perpendicular to the spacecraft's track ( $V_y$ ) in km/s. Here, positive is anti-sunward and negative is sunward. The region of anti-sunward flow at the highest latitudes is clearly visible with the returning sunward flow on either side of it at lower latitudes. The change in signs here denotes the locations of the convection reversal boundary for this pass. The second panel shows the vertical ion flow perpendicular to the spacecraft's track ( $V_z$ ) in km/s. Here, positive is upward. The most notable feature in this panel is the upward and structured flow in the auroral regions just outside of the convection reversal boundaries. The bottom panel shows the integrated electrostatic potential calculated from this pass in kilovolts. The sinusoidal two-cell shape is clearly present here and the asterisks denote the locations of the maximum and minimum potentials along this pass. The maximum and minimum fall exactly at the convection reversal boundary. Below all three panels is a set of headings denoting the time of occurrence in universal time (UT) along with the coordinates of the spacecraft at that point in magnetic local time (MLT), invariant latitude (ILAT), magnetic latitude (MLAT), geographic latitude (GLAT), and geographic east longitude (GLON).

DBASE4 was designed to do the above analysis on a routine and automatic basis, and pass its output on to the MSM or any other operational model which needed these data. In outline form, DBASE4 functions as follows: First, it takes the four-second averaged arrays of the vertical and horizontal ion flow data for one-half orbit (equator crossing to equator crossing). These flows are generally steady and close to zero up to about 50° magnetic latitude. They begin to show more structure poleward of this latitude (Figure 3). DBASE4 searches to find appropriate endpoints on either side of the polar regions where the flows are steady and close to zero. Once those endpoints have been determined, the routine averages the flows at either end for each flow component, and removes that average from all the flow data points in that array. This effectively zeroes the baseline of the flow data for each component. These reset data arrays are combined with the Earth's magnetic field to calculate the electrostatic potential from the starting point to the stopping point. The potential starts at zero and, ideally, should return to zero at the stopping point. However, this is rarely the case. Since it takes the spacecraft 15 to 22 minutes to cross the region being measured, there is enough time for the flow pattern to change during the crossing. Generally if the pattern is steady, the potential curve will return to near zero at the stopping point. But if the pattern has changed during the pass, then the potential will be far from zero at the stopping point. Thus, the potential at the stopping point, or "offset" as it is referred to, serves as a crude indicator of the quality of the procedure for each pass. The program uses the offset to perform a linear correction to the potential distribution to "force" the stopping point back to zero.

The program takes this corrected distribution and finds the maximum and minimum points on it to determine the observed potential drop. It then examines the positions of the maximum, the minimum, and the zero potential point and compares them to where the location of the zero potential point would be for each of the three Heppner-Maynard mod-



WILLIAM B. HANSON CENTER FOR SPACE SCIENCES

THE UNIVERSITY OF TEXAS AT DALLAS

Figure 3. This is a data plot of an entire orbit of DMSP ion density data and ion flow data. The plot begins at the equator on the northbound leg of the orbit, goes over the northern polar regions, recrosses the equator heading southward, crosses the southern polar region, then ends at the equator on the next northbound leg. The top panel is the ion density data taken from the scintillation meter and presented on a log scale going from  $10^2$  to  $10^6$  ions per cubic centimeter. The next three panels show the ion flow data in the x-direction (parallel to the spacecraft's velocity vector, data from the RPA), y-direction (horizontal perpendicular to the spacecraft's velocity vector, data from the DM), and z-direction (vertical perpendicular to the spacecraft's velocity vector, data from the DM). (Note: since this is an F8 plot, there are no  $V_x$  data available to plot for this pass.) The point of this figure is to show the large ion flows seen in the data in the polar regions as opposed to the steady, near-zero flows seen outside of those regions. It should also be noted that the flows outside of the polar regions are not always exactly zero; thus, it is necessary to rezero the baseline for the flows for each pass prior to analysis.

els. If the observed zero potential point is close to one of the three models, then the program declares the pattern of this pass to be a fit to that particular model. Since the orientation of any satellite would rarely carry it through the region of the absolute maximum and minimum potentials, the program then compares where the spacecraft's track passed through the ideal Heppner–Maynard pattern, and calculates how much the observed maximum and minimum should be corrected to get the “true” potential drop. The program then outputs a “shortfile” which contains the locations and magnitudes of the maximum and minimum, the location of the zero point, the model number of the Heppner–Maynard pattern, the correction factors for the maximum and minimum, and several other parameters. It also outputs a “longfile” which contains the flow and potential data for each four second period for the entire half orbit. (The potential data are set to zero at all the points outside of the endpoints.) See *Hairston and Heelis* [1993] for the format of the “long” and “short” files.

Of course, not all the passes neatly fit the three southward IMF Heppner–Maynard patterns. If the observed potential drop is less than 40 kV in spite of the fact that the spacecraft passed above 75° magnetic latitude, then that pass is judged to be a northward IMF pass. In such a case, there is no attempt to match this pass to the three Heppner–Maynard patterns and the program simply outputs the longfile and shortfile. If the total observed potential drop was less than 10 kV and the spacecraft did not go above 75° magnetic latitude, then this was marked as a pass which only skimmed the edge of the polar region and one for which a pattern cannot be determined. Again, the program would then skip the pattern analysis and simply output the longfile and shortfile. If only one cell was observed (either no maximum or no minimum was observed) then the spacecraft only passed through a single cell and cannot match it to one of the Heppner–Maynard patterns. Again, the program will skip the pattern analysis and output the longfile and shortfile.

There are also cases where the pattern analysis itself fails. If one of the potential correction factors based on the chosen Heppner–Maynard pattern was excessively large (here the cutoff was originally set at greater than 10.0) or if the zero point was too far into the nightside to classify it unambiguously as one of the three patterns, then a model number indicating that failure was chosen and the program would output the longfile and shortfile. Last, there were some cases where either the program was unable to determine suitable endpoints or there was a large (greater than two minutes) data gap in the telemetry during this pass. In these cases, there would be no attempt to calculate the potential distribution and these were referred to as “null passes”. Instead, a shortfile of all zeroes (except for the identification number for the pass, referred to as the SFINDEX number) would be output along with a longfile which contained the flow data arrays, but zeroes for all the elements of the potential array.

The code for the model number in shortfiles produced by DBASE4 is:

- 0 – northward IMF ( $\Delta \text{PSI} < 40 \text{ kV}$ , highest magnetic latitude point  $> 75$  degrees)  
or else a null pass when all other elements in the shortfile are also zero
- 1 – HM model BC
- 2 – HM model A
- 3 – HM model DE
- 4 – unusable (zero occurred in far nightside or else pattern is too distorted to classify unambiguously)
- 5 – skimmer (unusable— $\Delta \text{PSI} < 10 \text{ kV}$ )
- 6 – unusable (either observed maximum or minimum potential was zero)
- 7 – unusable (one of the corrections greater than 10 or negative, pattern likely too distorted to classify unambiguously)

Only models 0 (northward IMF) through 3 were used by the MSM. The other model numbers were only used for analysis of the DBASE4 routine and other research projects. Once a pass was finished, DBASE4 would continue on to analyze the next polar pass.

### 3. Building the DBASE4 Database

Once the code for DBASE4 had been finalized, the next step was to apply it to analyzing the stored set of DMSP telemetry. Doing this would provide us and the rest of the scientific community with a set of reduced data which could be used for further analysis and development of the improved versions of the DBASE code. The processing procedure entailed running a 10-day telemetry set through the DBASE4 code and producing one longfile for each one-half orbit and one shortfile for each 10-day telemetry set. (The choice of a 10-day increment was based on the 9-track tapes of telemetry provided to us by Phillips Laboratory. Each month was broken into three parts: 1 – 10, 11 – 20, and 21 – end, so the final section could vary from eight to eleven days in length. For F11 onward the telemetry is broken into two parts per month: 1 – 15 and 16 – end.) Following this initial procedure, the telemetry was run through a second program performing RPA analysis and placing those results in a datafile called an “R-file”. These “R-files” contained the flow data, satellite position, electron and ion temperature, scintillation data, ion density, and fractional composition of the ions (for periods where the RPA was operating) for each four seconds. These files are intended as a complement to the data in the longfiles. For the periods where there were no RPA data (such as most of F8’s lifetime and all of F9’s lifetime) the R-files were produced anyway to store all parameters other than those derived from the RPA data. Each R-file is one orbit in length spanning from the equator crossing on the northbound leg (ascending node) to the next equator crossing on the northbound leg. All the data were ultimately saved in the National Center for Supercomputing Applications’ Hierarchical Data Format (HDF) so that the reduced data could be stored onto CD-ROMs. The HDF is platform-independent, so the CDs can be read by any machine (VAX, Unix, PC, Macintosh, etc.) with the proper software.

Undertaking this data analysis was not a small task. Even in its reduced form, four

months of longfiles and R-files from a single satellite fill an entire CD. In general, we found that we could average processing one CD worth of data per week. As of the end of 1995, there were approximately 20 satellite-years worth of DMSP telemetry available. Processing this entire amount of telemetry would produce 60 CDs of reduced data and require over one year of fulltime work by the person overseeing the procedure. To date we have been able to process the entire F9 dataset (just over 4 satellite-years of data) and the F8 dataset up to the end of 1993 (6.5 satellite-years of data). This processing is an ongoing effort that should extend beyond the end of this contract. Ultimately, the entire DMSP dataset should be reduced and stored on CDs.

Simply having this huge reservoir of reduced data available is not useful if there is no way to examine that data easily. In the summer of 1995, we started work on developing a single program called PLOTDMSP which would allow a user to choose any R-file or long-file and then plot those data in whatever form the user chooses. Most of this work has been performed by an undergraduate student, Dorothy Chan, and one of our graduate students, Onder Kivanc, using PV-Wave software. Currently, the program allows the user to plot flow data (on either a polar dial or as x-y plots), ion densities, the polar potential curve, and ion and electron temperatures. Several of the figures in this report were produced with this program. It would be beneficial to provide such a graphic interface to the data to all users through appropriate internet access.

As part of our ongoing efforts throughout this contract period, we have provided parts of the reduced dataset to various outside researchers for scientific collaboration. The list of persons who have received data from us includes: Lt. Col. Delores Knipp, US Air Force Academy; Dr. Barbara Emery, NOAA; Dr. Gang Lu, NOAA; Dr. Phillip Anderson, Aerospace Corp.; Dr. Margaret Chew, Aerospace Corp.; Dr. Pat Newell, Applied Physics Laboratory; Dr. Geoff Crowley, Applied Physics Laboratory; Dr. Ennio Sanchez, was at Applied Physics

Laboratory, now at SRI; Dr. Richard Wolf and Dr. John Freeman, Rice University; Dr. Patricia Reiff and Ben Boyle, Rice University; Dr. Robert Clauer, University of Michigan; Mariko Satoh, Nagoya University, Japan; Dr. Nicola Fox, was at Imperial College, London, England, now at Goddard Space Flight Center; Dr. Alan Rodgers and Dr. Mike Pinnock, British Antarctic Survey, Cambridge, England; and Dr. Vyacheslav G. Vorobjev, Polar Geophysical Institute at Murmansk, FSU. We have also provided DMSP data for numerous campaigns under the NSF's GEM and CEDAR programs.

#### **4. Revisions of the Output of DBASE4 to Suit MSM Operations**

One of the primary purposes of the development of DBASE4 was to provide inputs to the Magnetospheric Specification Model (MSM) operational code being run by the Air Weather Service. The primary requirements were that it produce a value indicating which of the three Heppner–Maynard patterns the pass most closely resembled (or a northward IMF pattern), the hemisphere in which this pass occurred, and a corrected cross cap potential drop based on the observed potential drop and the chosen pattern. The shortfiles output by DBASE4 contained all these data along with more data which were used for scientific and developmental analysis. It was assumed that as the MSM evolved, it would be able to incorporate these extra data as well.

In the fall of 1994 under the direction of Captain Devin Della–Rose of 50th Weather Squadron the procedures were modified to produce output in a format that could be directly fed into the MSM instead producing a shortfile. This format would be based only on the required data for the MSM along with some selection rules developed by the Rice University team which had written the MSM. An upgraded version of the section of the code was delivered to 50th Weather Squadron in January 1995. The new output for each pass took the form of:

YYYY DDD.FFF PCP.FF sHP

where

- YYYY is the four-digit year of the pass.
- DDD.FFF is the day of year number and a three digit-fractional day value (based on the time at the equatorial crossing at the beginning of a one-half orbit pass).
- PCP.FF is the corrected crosscap potential drop in kilovolts to two places after the decimal
- sHM is the Heppner-Maynard model number (1, 2, or 3) with "s" standing for a plus or minus sign indicating a northern or southern polar pass respectively.

The major change requested by the Rice University researchers was that for northward IMF cases (model number 0), the output model number be reset to 2 (Heppner-Maynard pattern A) for the MSM's use. They discovered that using the model 2 pattern during northward IMF conditions gave adequate results for the MSM. Also, passes that returned any of the higher model numbers (4 through 7) were to be excluded. The code excludes any passes where the total potential drop was less than 20 kV or where the offset divided the total potential drop exceeded 0.80. For these cases, no data are returned for that pass and the program moves on to the next pass.

At the Quarterly Review Meeting in Spring 1995 it was determined that the corrected potential drops produced by DBASE4 were frequently extremely large and unrealistic. Figure 4 shows one month (September 1990) of observed potential drops from F8 (the solid line) and the DBASE4 corrected potential drops (dotted line) in the southern hemisphere. F8 was chosen since its orbital orientation is closest to the dawn-dusk line and thus should produce the most accurate corrected values. The month of September was chosen since it is centered around an equinox, so conditions should be roughly the same in both polar hemispheres. The first thing to notice in this figure is that the observed potential drop falls

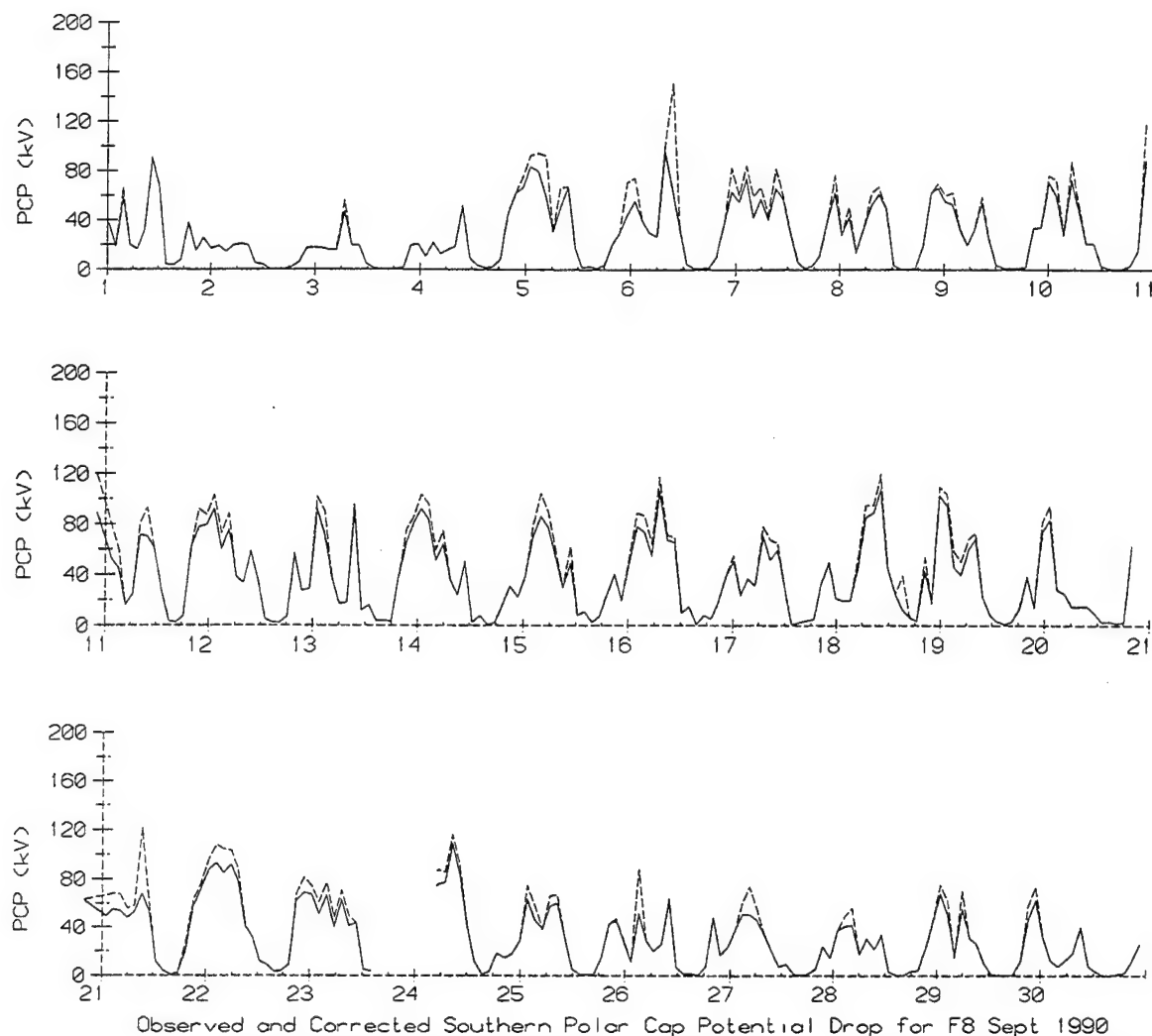


Figure 4. This is a plot of the measured and estimated polar cap potential drop as seen by F8 in the southern hemisphere for the month of September 1990. The solid line is the observed drop and the dotted line is the estimated actual drop based on the Heppner-Maynard models. Note that the estimated values are generally no more than 15% above the observed potential drop. The regular drop to zero potential in each day's data is a result of the spacecraft's groundtrack moving outside of the polar region as the Earth rotates underneath it once a day. Thus, these are the periods where the spacecraft only skims the edge of the polar region.

to near zero on a regular basis once a day. This is caused by the tilt of the dipole axis where these are the passes which occur when the spacecraft only skims the edge of the polar cap region. The second thing to notice is that (skimmer passes aside) there is a great variability in the total potential drop and that changes in magnitude can occur on very short time scales (less than an hour). Finally, notice that the corrected potentials seem reasonable here, rarely exceeding more than 1 – 15% above the observed potential drops.

Figure 5 shows the same period of F8 data for the northern hemisphere. For the northern passes F8 never leaves the polar cap region, so any decreases in the observed potential drop should reflect actual changes in the ionosphere. Again, the potential drop can be seen to be quite variable on short time scales. But while the observed potential drops (solid line) are comparable to those seen in the southern hemisphere, the corrected values (dotted line) are wildly exaggerated and most certainly not real.

Why should there be such a difference between the corrected values in one hemisphere over the other? The key lies in Figure 6 which shows the extent of the ground tracks of F8 for one day in each hemisphere. In the southern hemisphere all the passes occur on the dayside of the dawn–dusk line while most of the passes in the northern hemisphere occur on the nightside of that line. In general, the distribution of the potential along the convection reversal boundary (which forms the basis of the correction factors for DBASE4) is well defined on the dayside. So it is not surprising that the corrections for the southern hemisphere turn out to be quite reasonable. However, the potential distribution along the nightside of the convection reversal boundary is not as well understood and likely a more variable function than presented in the three Heppner–Maynard models. In this case the correction factors for the northern hemisphere (nightside) passes should be less reliable and more prone to overexaggeration.

We performed a statistical breakdown of the sizes of the correction factors. The analy–

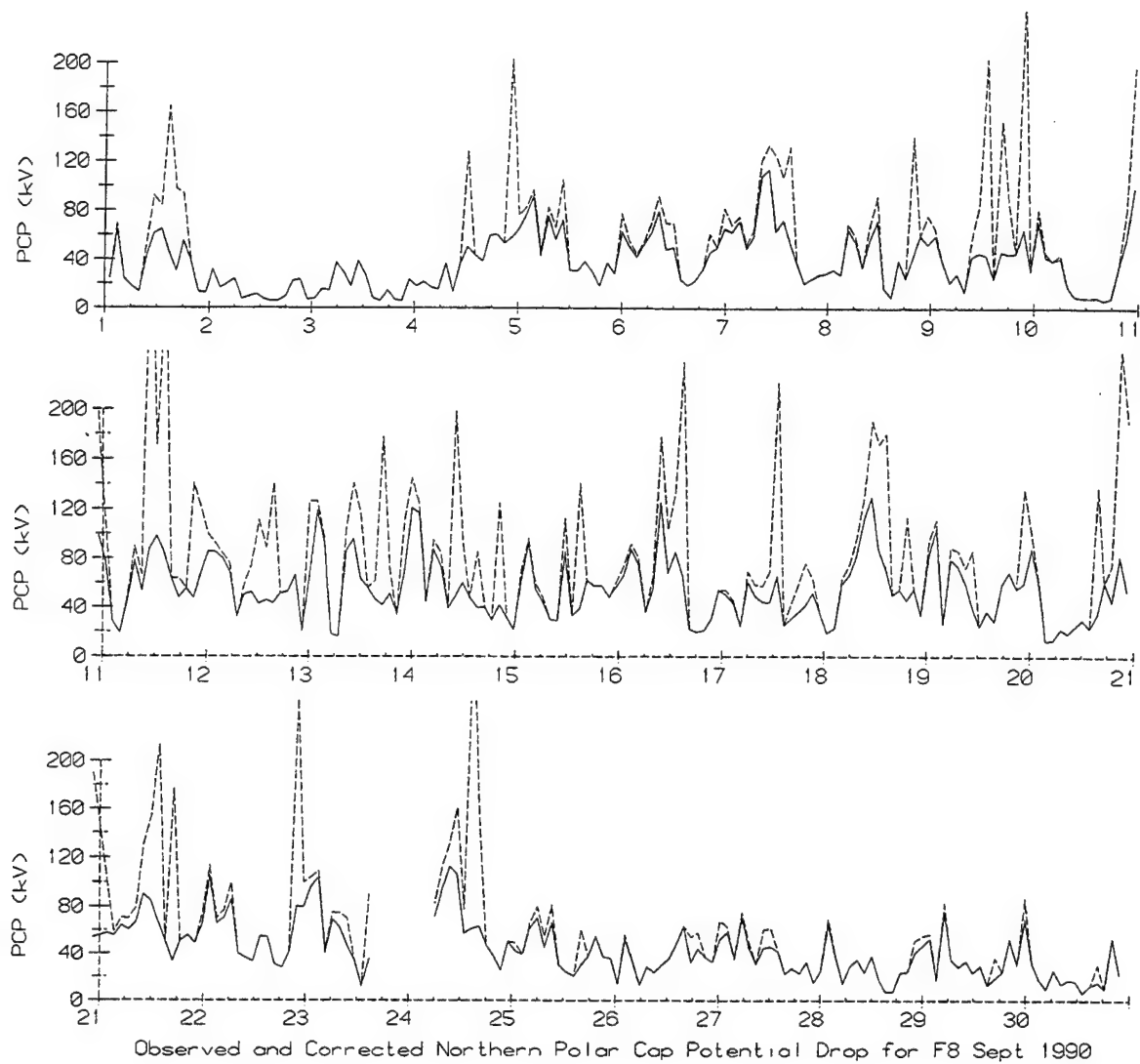


Figure 5. This shows the measured and estimated polar cap potential drop as seen by F8 in the northern hemisphere for the month of September 1990. Like Figure 4, the solid line denotes the observed potential drops and the dotted line denotes the estimated drops based on the Heppner-Maynard patterns. It is obvious from this plot that the estimated drops are exaggerated, and the reasons for this are discussed in the text.

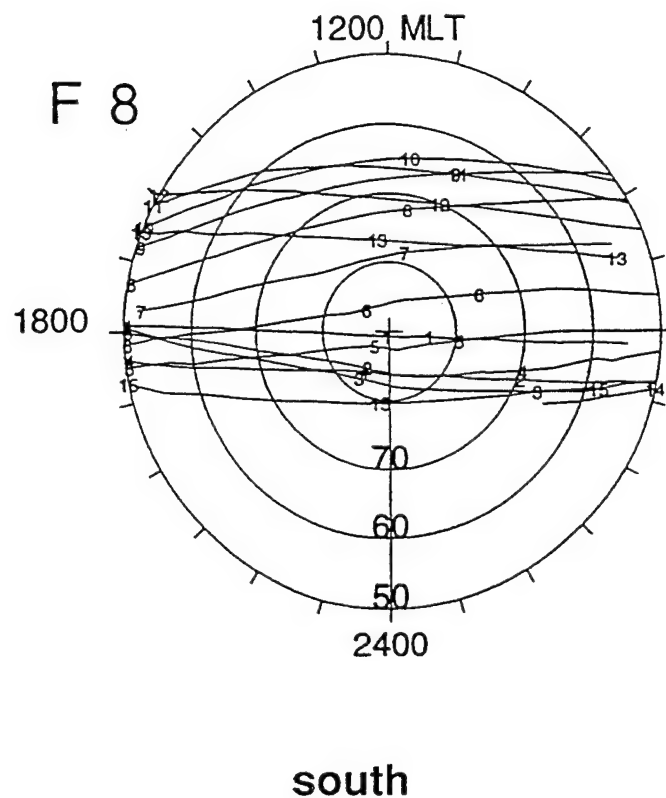
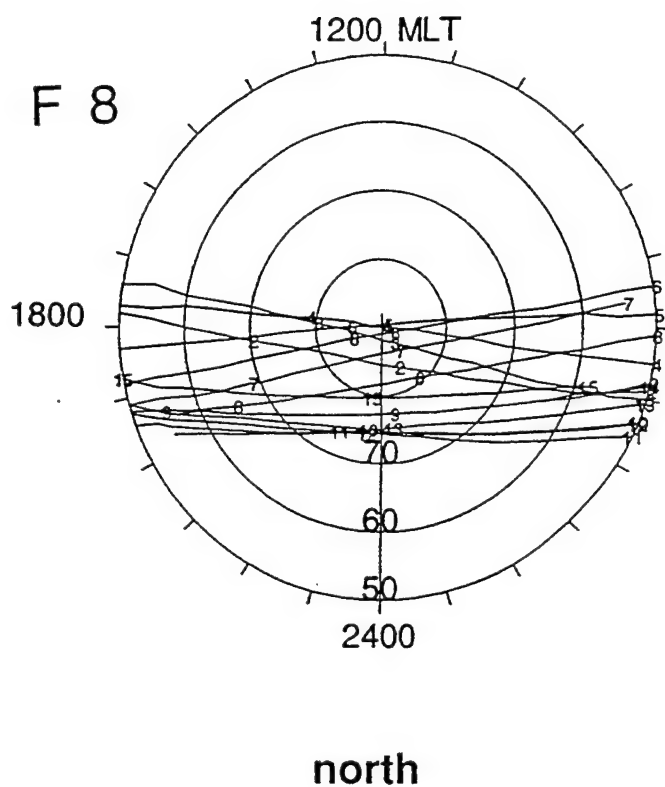


Figure 6. These plots show the groundtracks in magnetic local time / magnetic latitude coordinates of F8 for one day in each hemisphere. The change in the tracks is caused by the rotation of the Earth's magnetic dipole relative to the inertial frame of the spacecraft's orbit. The northern hemisphere is on the left and shows that most of the passes occur on the nightside of the dawn-dusk line. The southern hemisphere is on the right and shows that most of the passes occur on the dayside (plus the fact that about one-quarter of them fall outside of the polar cap region).

sis used the four months of June, August, September, and December of 1990 for F8. This insured that all seasonal conditions would be covered. The results of the percentage size of the total correction divided by the total observed potential drop are shown below.

**Table 1**

correction of 0 – 10%	30.49% of corrected passes
correction of 10 – 20%	20.90% of corrected passes
correction of 20 – 30%	10.22% of corrected passes
correction of 30 – 40%	4.33% of corrected passes
correction of 40 – 50%	3.25% of corrected passes
correction of 50 – 60%	2.63% of corrected passes
correction of 60 – 70%	2.17% of corrected passes
correction of 70 – 80%	2.48% of corrected passes
correction of 80 – 90%	2.17% of corrected passes
correction of 90 – 100%	2.32% of corrected passes
correction of over 100%	19.20% of corrected passes

(note: total slightly exceeds 100% because of rounding errors)

From the above table, it is clear that slightly more than half the corrected passes had corrections of less than 20% of the observed total potential drop. Based on these results it was agreed by the Rice researchers and the UTD researchers that the algorithm for the corrected potential drop would be capped at 20%. Thus the output for MSM now checks the total corrected potential drop and, if it is more than 20% above the observed potential drop, then it resets it to exactly 20% above the observed potential drop. This revision of the output code has been incorporated into the code delivered with this report. However, it is not clear that this cap has been implemented into the operational code at 50th Weather Squadron. "Block 4a" is the part of the program that outputs the shortfile data and the MSM format data. In the version of the program delivered with this report, the entire code in this block has been commented out. The end user (Phillips Laboratory or 50th Weather Squadron) can easily "uncomment" either section of the code to choose the version (MSM or

shortfile) of the output they wish to use.

The problems with the "overcorrection" of the potential drop clearly point out the limitations of using only the three Heppner–Maynard patterns as a basis for modeling the ionospheric convection patterns. Even a casual inspection of the DMSP potential data show that the overall patterns of the ionospheric convections are quite variable and frequently much more complex than can be accounted for by only three averaged patterns. While the Heppner–Maynard patterns provide a good starting place for modelling effort, it is generally accepted that they are first–order models and that modelling of the distribution of the potential along the nightside portion of the convection reversal boundary still requires much more work. In order to provide better estimates of the total cross–cap potential drop and a more accurate characterization of the convection flow pattern, it will be necessary to develop newer and more sophisticated convection flow models. The DMSP database is an ideal dataset to use for developing such models, and we hope that future efforts by UTD and Phillips Labs will involve the development of these more sophisticated models.

## **5. Comparison of Heppner–Maynard Model Selection Results with Actual IMF Data**

Another question which was raised at the Quarterly Review in spring 1995 was: how well does the algorithm in DBASE4 which selects the three Heppner–Maynard pattern work when compared to the actual IMF data? Each of the three patterns is based on a particular, steady orientation of the IMF in the  $y$ – $z$  plane. Prior to the launch of the WIND satellite (which provides near continuous monitoring of the solar wind in front of the Earth's magnetosphere) the only solar wind data available came from the IMP–8 spacecraft. However, those data were sporadic and usually delayed months (if not years) before they were released for use. Early in the development of DBASE4, it was hoped that ultimately the de-

rived potential distribution might be used to work backwards to estimate the IMF orientation based on the observed pattern, thus providing a pseudo-solar wind monitor. At this point the database had grown large enough and the amount of historical IMP-8 data released was sufficient that a comparison could be performed.

If the magnitudes of the cross-cap potential drop is plotted as a function of the orientation of the IMF in the  $y$ - $z$  plane, then ideally something like Figure 7 should appear. When the IMF is oriented northward (the  $0^\circ - 90^\circ$  and  $270^\circ - 360^\circ$  sectors) then there is little coupling between the IMF and the magnetosphere, so the potential drop should be relatively small (rarely more than 40 kV). When the IMF is oriented southward ( $90^\circ - 270^\circ$  sectors) then the IMF does couple easily with the magnetosphere and the potential drops are larger. The largest drops would occur when the IMF was oriented due southward ( $180^\circ$ ). Since the magnitude of the potential drop is a function of the magnitude of the IMF and the solar wind speed as well as the orientation of the IMF, then there will be a scatter in the data points for any given IMF orientation. In general, the model 1 patterns should fall in the  $90^\circ - 180^\circ$  sector, the model 2 patterns should fall in the  $180^\circ - 225^\circ$  sector, and the model 3 patterns should fall in the  $225^\circ - 270^\circ$  sector, along with some overlap at the edges. Note that this is based on the patterns in the northern hemisphere. The same patterns occur in the southern hemisphere except that the sign on the  $B_y$  is reversed. Thus, for the following analysis, the results from the southern hemisphere have been flipped about the  $180^\circ$  point before being plotted onto the graphs.

The same shortfile datasets of F8 data from June, August, September, and December 1990 that were used above were also used for this analysis. First, all the passes were examined and only those where the hourly IMF averages during the pass and during the previous hour showed that the IMF clock angle (in the  $y$ - $z$  plane) were in the same quadrant were selected. While there is a large variability in the IMF clock angle which is hidden by

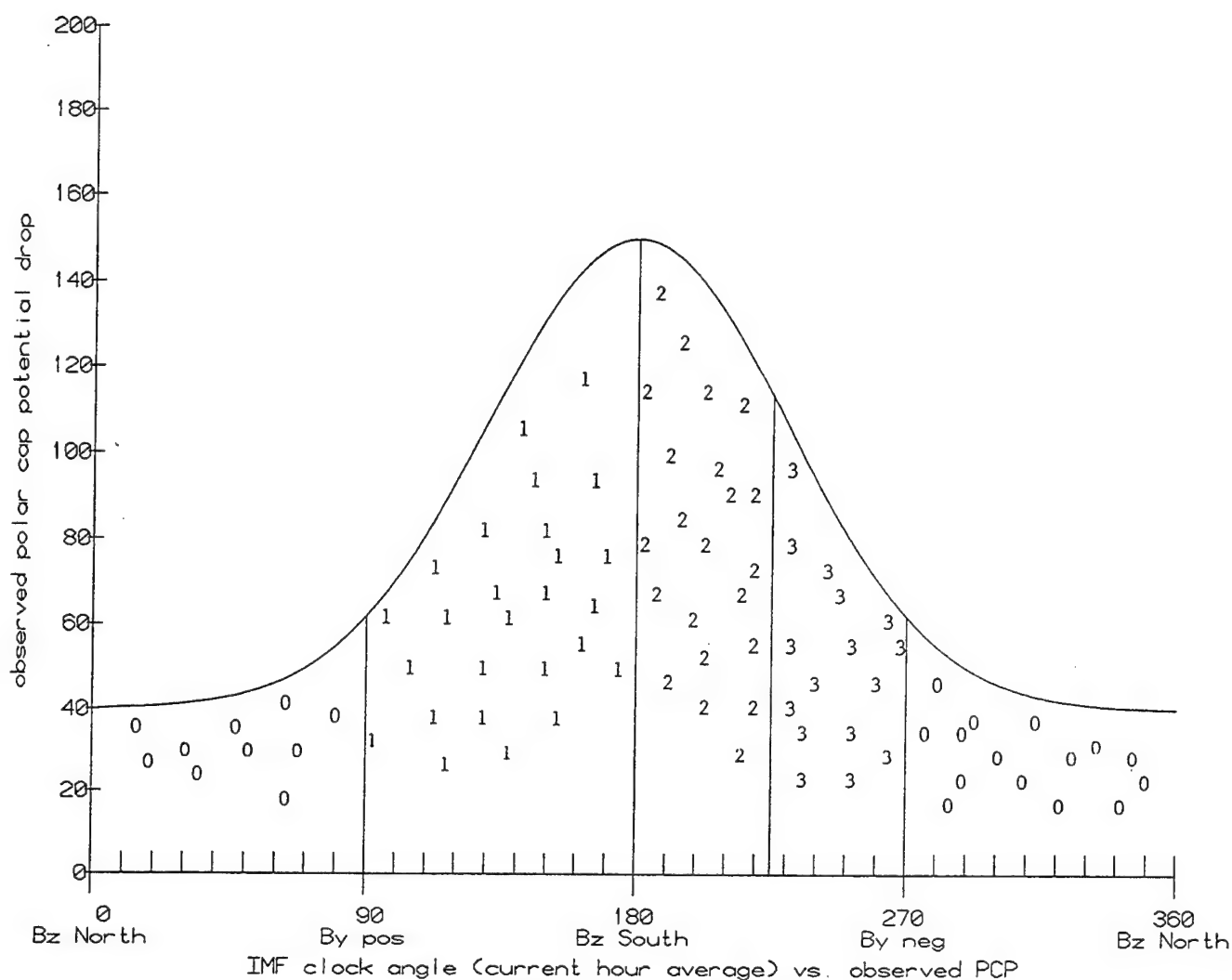


Figure 7. This is an idealized distribution of the polar cap potential drop magnitudes plotted against the existing IMF clock angle. The numbers represent the model number of the pattern for the pass plotted at that point. Because of variations in the conditions of the ionosphere and the solar wind, there will be some scatter in the magnitude of the potential drops. But in general the largest values will be at times when the IMF is most strongly southward ( $180^\circ$ ) and smallest when the IMF is most strongly northward ( $0^\circ / 360^\circ$ ). In the ideal case, all the Heppner – Maynard models (1–3) would fall neatly into the three bins between  $90^\circ - 270^\circ$ , and all the passes in the remaining two quadrants would be classified as northward IMF cases (model 0).

the hourly averages, this selection rule gives a rough guide to times where the IMF was steady enough for the pattern to become established and remain stable in the ionosphere. Next, the magnitude of the cross-cap potential drops were plotted as a function of the IMF clock angle during the hour of the pass. However, a better correlation was found by plotting the potential drops as a function of the IMF clock angle during the hour prior to the pass. This correlation is reasonable since there is some time lag between changes in the IMF orientation and the establishment of the convection pattern.

Figure 8 shows the potential drops derived for passes identified as model 0 passes (northward IMF cases). Clearly, most of the points do fall into the first and fourth quadrants (northward IMF) and are less than 40 kV. (The cutoff at 40 kV is an artifact of the analysis procedure; passes greater than 40 kV cannot be classified as a model 0 case.) There are some cases which fall within the middle two sectors, but those are likely cases when the magnitude of the IMF was relatively small in spite of being oriented southward.

Figure 9 similarly shows the potential drops for of all the passes which were identified as model 3 (Heppner–Maynard model DE:  $B_z$  southward,  $B_y$  extremely negative for north hemisphere / extremely positive for southern hemisphere) from this four-month sample. This pattern occurs relatively infrequently as shown by the sparse number of data points. However, they do appear only in the region around the  $270^\circ$  angle where they would be expected. Notice that some of them appear at angles slightly greater than  $270^\circ$ . This is consistent with the observations in *Rich and Hairston* (1994) that for cases of large magnitude  $B_y$  / slightly northward  $B_z$  there is still some weak coupling of the IMF to the magnetosphere and a two-cell convection pattern remains.

Figure 10 shows the potential drops derived for all the passes identified as model 2 (Heppner–Maynard model A:  $B_z$  southward,  $B_y$  negative for north hemisphere / positive for southern hemisphere) from this four-month sample. While the data points cluster in the

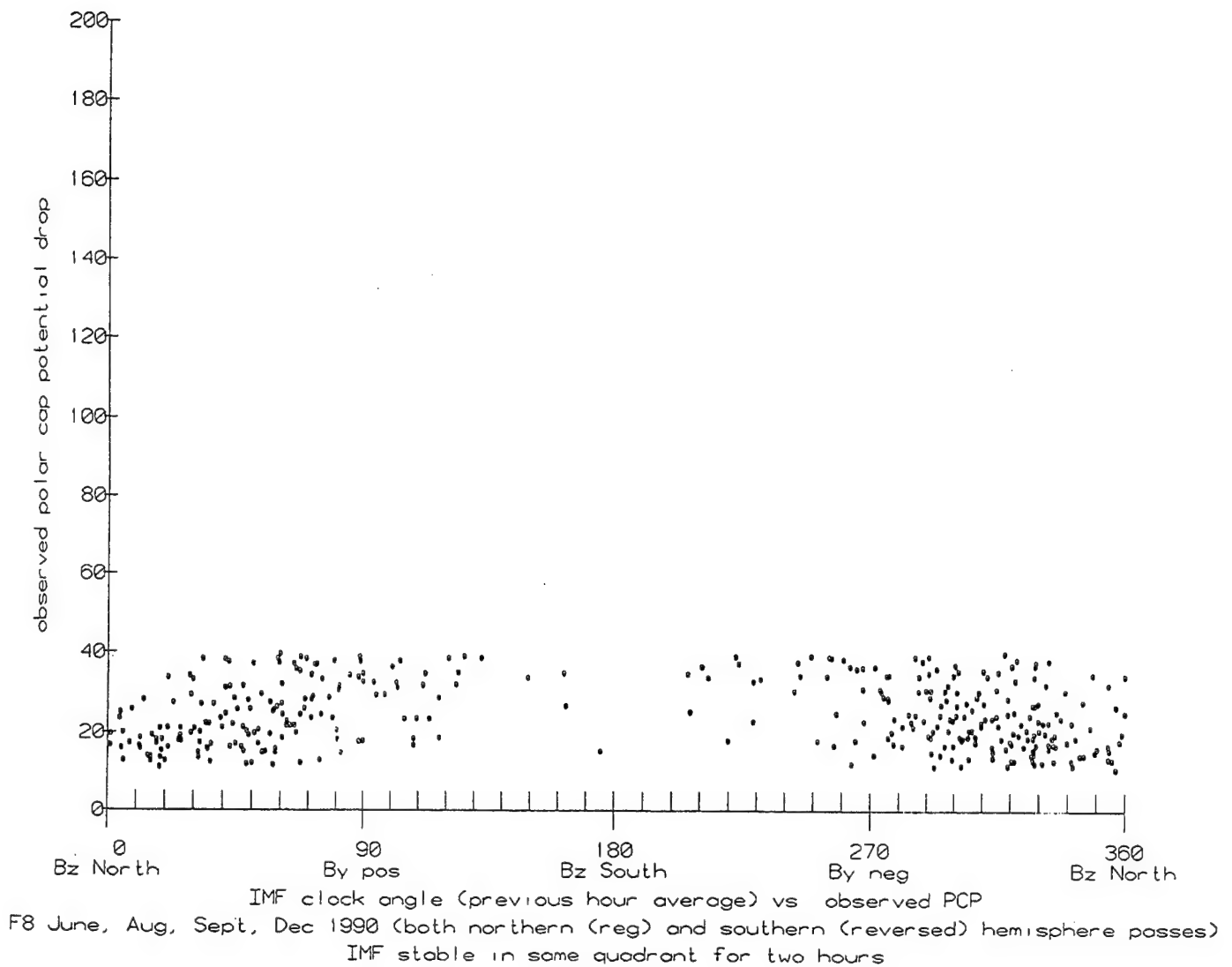


Figure 8. This shows the distribution of the polar cap potential drops as a function of the IMF clock angle for all passes identified as model 0 (northward IMF) after the IMF was steady in the same quadrant for two consecutive hours. These data come from F8 during the months of June, August, September and December 1990. While most of the data points cluster in the first and fourth quadrants as expected, there are a few which appear in the the middle two quadrants.

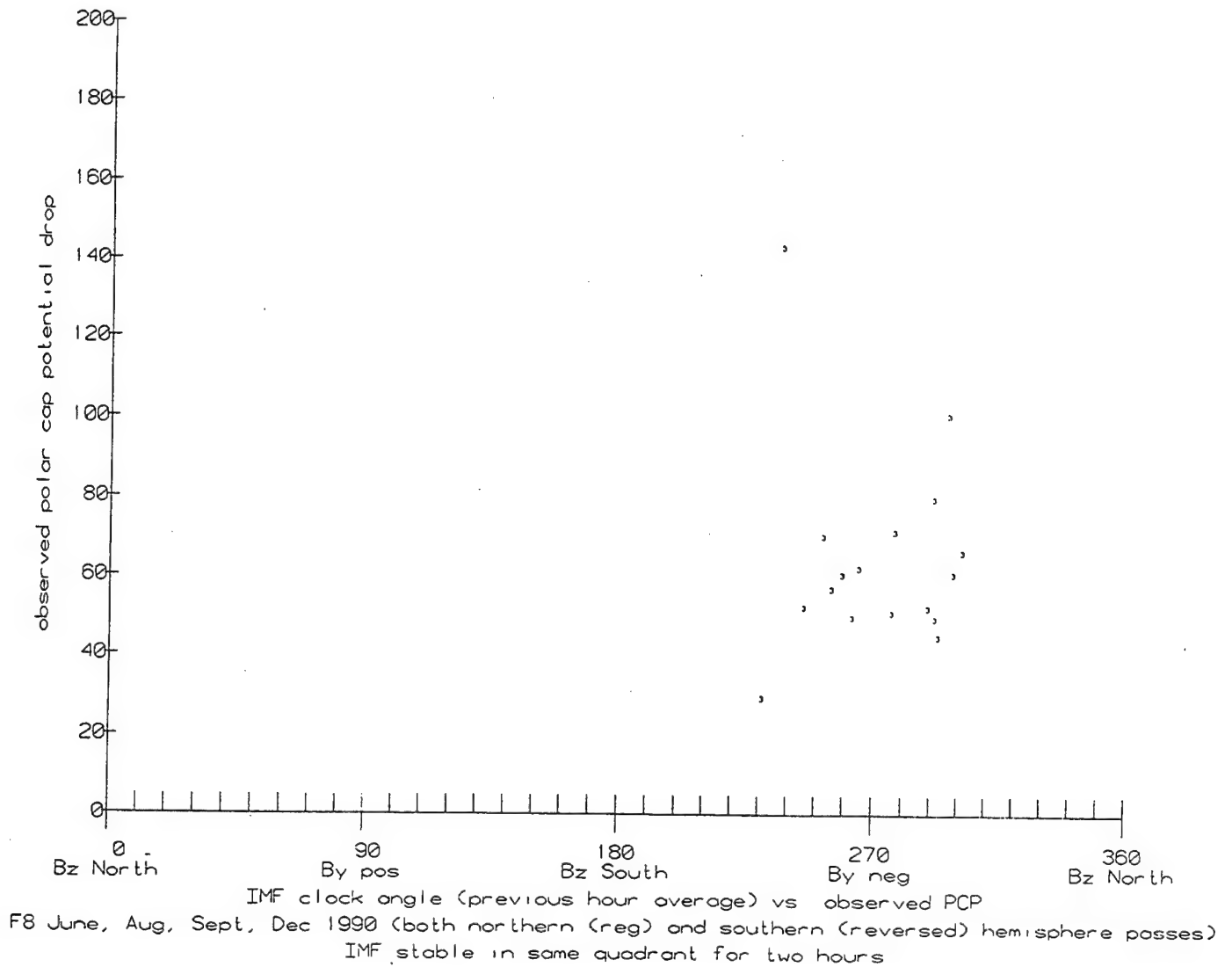
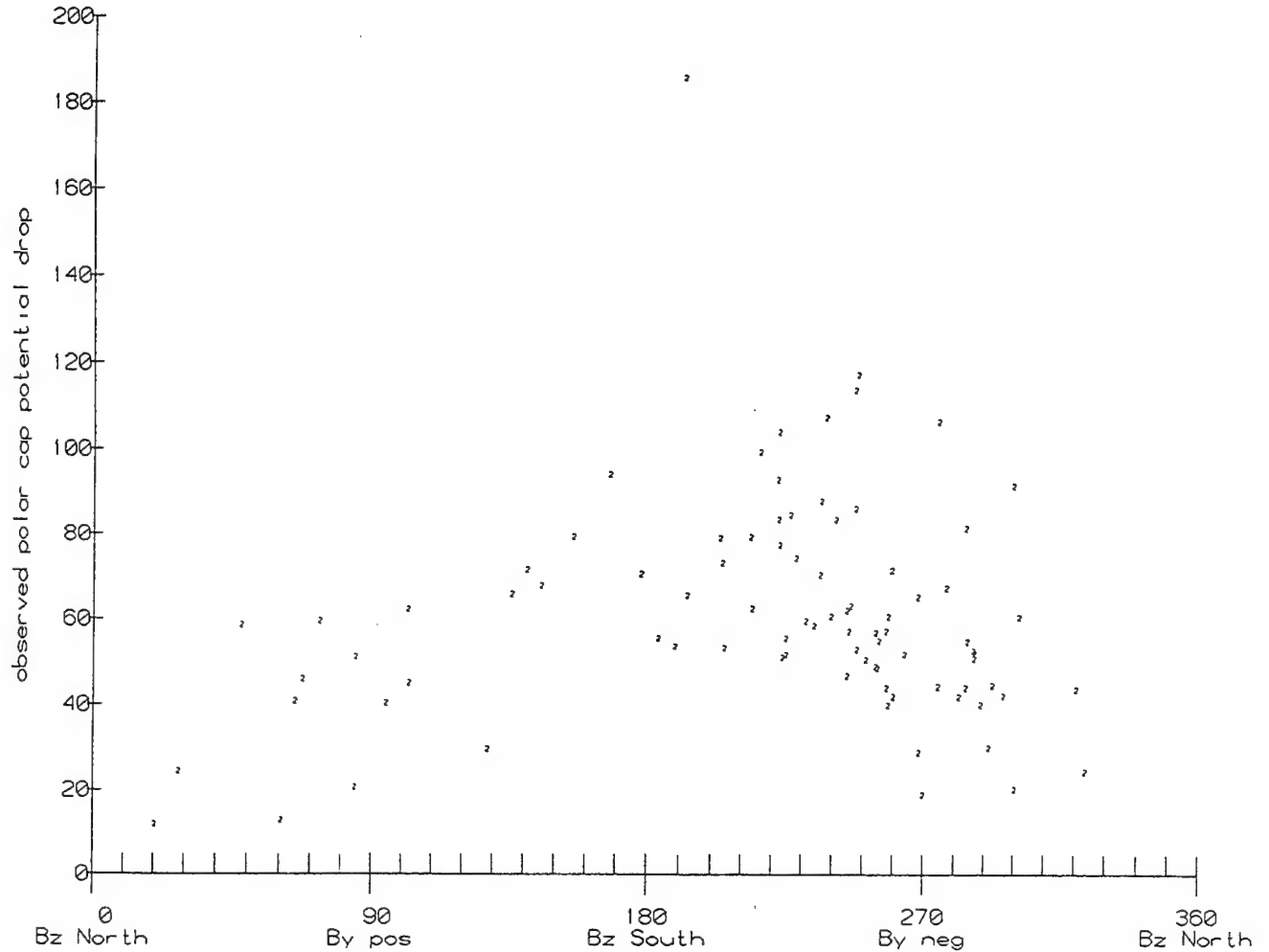


Figure 9. This shows the distribution of the polar cap potential drops as a function of the IMF clock angle for all passes identified as model 3 (Heppner-Maynard pattern DE, southward IMF /  $B_y$  very negative) after the IMF was steady in the same quadrant for two consecutive hours. These data come from F8 during the months of June, August, September and December 1990. All the datapoints cluster around the  $270^\circ$  clock angle, which is consistent with the predictions of the Heppner-Maynard model. (Note that the sign on  $B_y$  for the southern hemisphere passes has been switched before the clock angle was calculated.)



IMF clock angle (previous hour average) vs observed PCP  
 F8 June, Aug, Sept, Dec 1990 (both northern (reg) and southern (reversed) hemisphere passes)  
 IMF stable in some quadrant for two hours

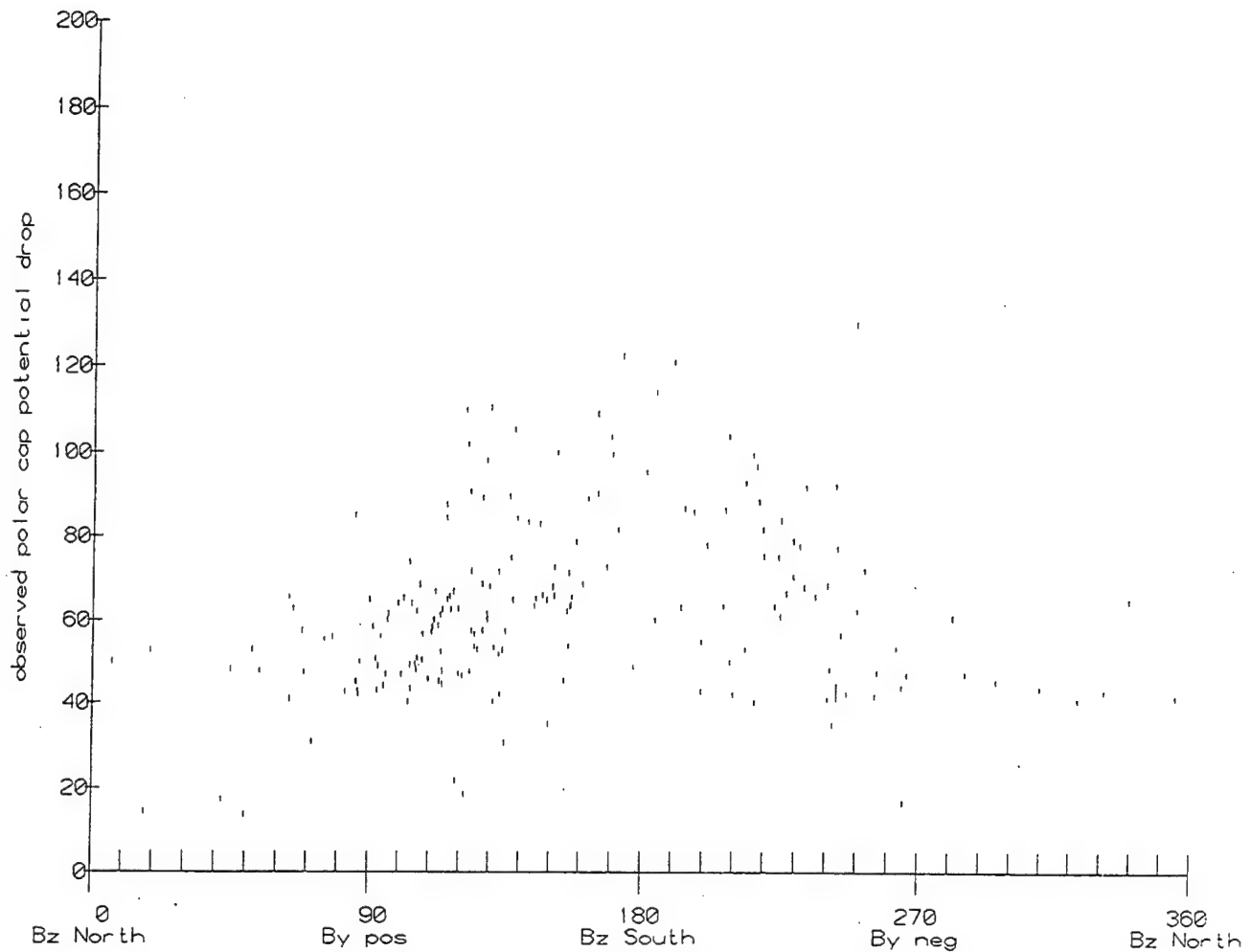
Figure 10. This shows the distribution of the polar cap potential drops as a function of the IMF clock angle for all passes identified as model 2 (Heppner-Maynard pattern A, southward IMF /  $B_y$  slightly negative) after the IMF was steady in the same quadrant for two consecutive hours. These data come from F8 during the months of June, August, September and December 1990. While the data points here do show some clustering in the  $180^\circ - 270^\circ$  region as predicted by the Heppner-Maynard model, an equal number are spread out through the other three quadrants. (Note that the sign on  $B_y$  for the southern hemisphere passes has been switched before the clock angle was calculated.)

third quadrant ( $180^\circ - 270^\circ$ ) as expected, the surprise here is that there are data points in all four quadrants. In other words, patterns which match the Heppner–Maynard model A are occurring during all possible IMF orientations.

Figure 11 shows the potential drops derived for all the passes identified as model 1 (Heppner–Maynard model BC:  $B_z$  southward,  $B_y$  positive for north hemisphere / negative for southern hemisphere) from this four-month sample. Again, the results are similar to those seen for model 2 data. While the data points clusters in quadrant 2 ( $90^\circ - 180^\circ$ ) this time as would be expected, again there are data points in all four quadrants. So, like model 2, model 1 patterns are not limited to any one region of IMF orientation.

Combining the data points from all four model choices produces Figure 12 which, in overall shape, matches the expected distribution in Figure 7 quite nicely. The surprise comes in the wide variety of IMF orientations where models 1 and 2 appear. It should be emphasized here that there is no problem with the model identification algorithm. Examination of the individual passes show that the correct pattern was indeed selected. The point here is that these patterns are not as strongly tied to the IMF orientation as was previously thought.

The convection patterns observed in the polar ionosphere are a product not only of the IMF orientation, but of the recent history of the IMF and the polar ionosphere. If the IMF only changed on very long time scales and the ionosphere reacted immediately to those changes, then modelling the patterns as a function of the IMF clock angle would be a straightforward task. In reality, however, the IMF is a rapidly changing input for most of the time. Also the ionosphere–magnetosphere system apparently displays some inertia, and a finite time is required to respond to a change in the IMF and establish a new convection pattern (*Hairston and Heelis, 1995*). Couple these facts together and it becomes obvious that the pattern at any given time is going to be a complicated result of several factors.



IMF clock angle (previous hour average) vs observed PCP  
 F8 June, Aug, Sept, Dec 1990 (both northern (reg) and southern (reversed) hemisphere passes)  
 IMF stable in same quadrant for two hours

Figure 11. This shows the distribution of the polar cap potential drops as a function of the IMF clock angle for all passes identified as model 1 (Heppner–Maynard pattern BC, southward IMF /  $B_y$  positive) after the IMF was steady in the same quadrant for two consecutive hours. These data come from F8 during the months of June, August, September and December 1990. While the data points here do show some clustering in the  $90^\circ - 180^\circ$  region as predicted by the Heppner–Maynard model, a nearly equal number appear in the  $180^\circ - 270^\circ$  quadrant and a few more appear in the northward IMF quadrants. (Note that the sign on  $B_y$  for the southern hemisphere passes has been switched before the clock angle was calculated.)

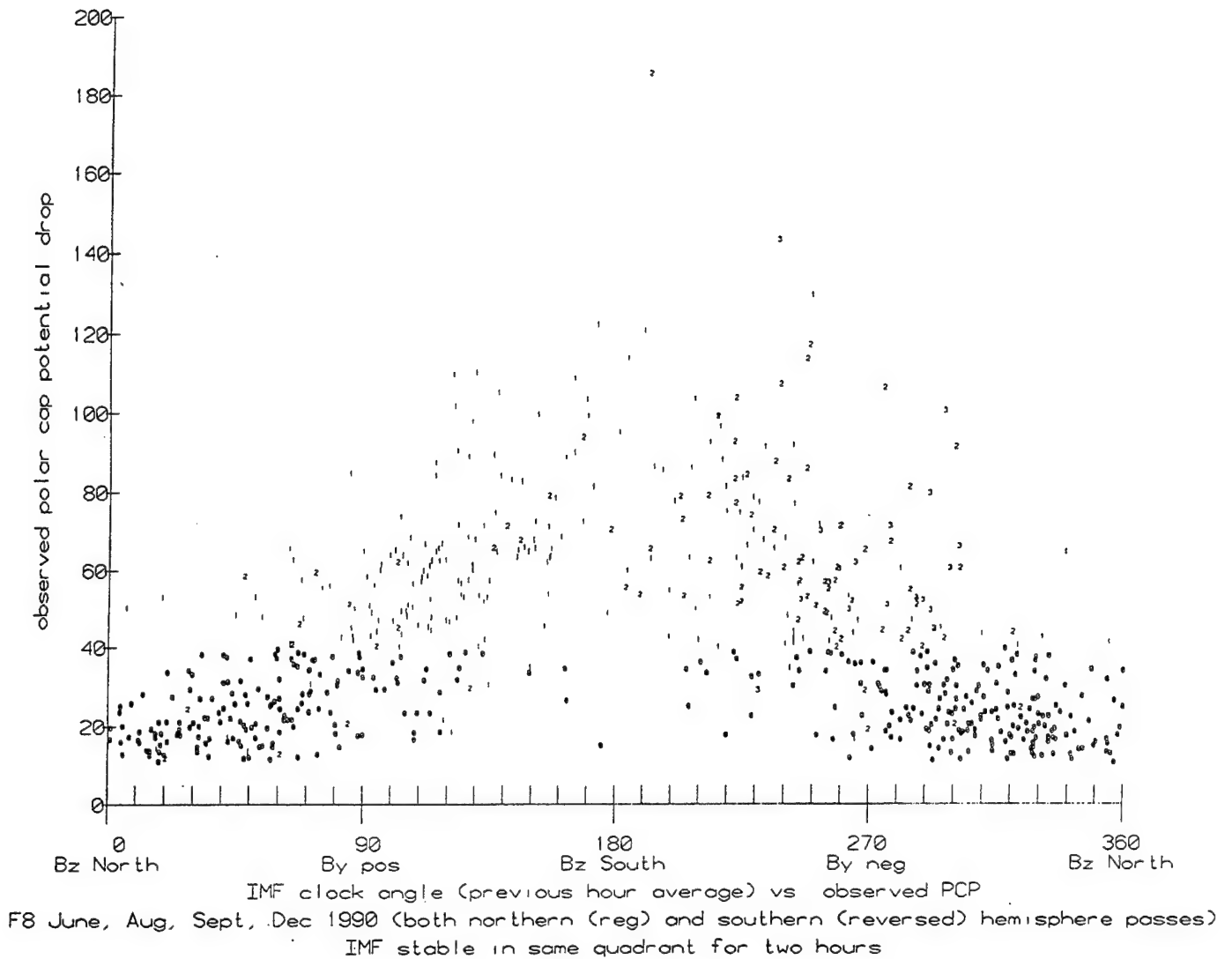


Figure 12. A combination of the data from Figures 8 through 11. Except for the wide distribution of the models 1 and 2 through all the IMF clock angles, the plot does make a fair match to the idealized case presented in Figure 7.

Individual passes which appear to the algorithm as models 1 or 2 (a steady state model) may in fact be intermediate states seen as the convection pattern is changing. Or passes which are identified by the algorithm as models 1 or 2 during times of northward IMF may actually be such patterns which have not yet decayed away despite the change in the IMF orientation.

This work points out the need for major improvements in the overall pattern identification processes if space weather forecasting is to become a reality. The current operational algorithms can only give this limited match to the three Heppner–Maynard patterns and make no effort to analyze the recent history of either the polar ionosphere or the IMF. However, a truly workable and reliable algorithm will have to incorporate the past history of the ionosphere, the IMF, and more sophisticated models of the convection flow patterns in order to give outputs of the quality necessary to model and forecast the conditions of the ionosphere and magnetosphere accurately. Such work was beyond the scope of this just-completed three year contract. However, with the growing size of the DMSP database and the current availability of the solar wind data from the WIND spacecraft, a more sophisticated set of convection flow models and algorithms for identifying them are now possible. It is hoped that work on such a modelling effort will be undertaken in the future.

## **6. Revision of the Origin Locator Algorithm in DBASE4**

In the model analysis portion of DBASE4, the locations of the maximum and minimum potentials are fit to a circle that represents the convection reversal boundary. The location of the zero potential point relative to this circle is used to determine which, if any, of the Heppner–Maynard patterns the pass most closely represents. The radius of this new circle is the average of the two distances from each of the extrema to the origin of the magnetic latitude / magnetic local time coordinate system, and the origin of the new circle is generally

within the 80° magnetic latitude circle. The original code for performing the algorithm in Block 3F/G was based on an F8 dawn–dusk orientation for the DMSP orbit, but it would occasionally fail to process data from the noon–midnight orientation of F9. The original algorithm was simply based on the analytical geometry of the intersections of the two circles of the averaged radius centered on the maximum and minimum. A new algorithm was required to meet the more variable orbital local times of future DMSP spacecraft. The new algorithm is based on analytic geometry and the fact that the intersections of the two circles also lie on a line which intersects the midpoint between the locations of the maximum and minimum at right angles. The algorithm starts by converting the locations of the maximum and minimum to an x–y coordinate system and then by calculating the distances from the locations of the maximum and minimum to the origin (Figure 13a). (This x–y coordinate system is the same system used throughout “Block 3F/G” where the +x line is the 0600 MLT line, +y is the 1200 MLT line and one degree of magnetic latitude on these axes defines one unit of measurement in the x–y coordinate system.) The midpoint along the line between the maximum and minimum is easily obtained by taking the averages of the two x components and the average of the two y components. The x,y coordinates of the maximum and minimum are used to determine the slope of the line between them. The inverse of that slope is the slope of the line which intersects the midpoint at right angles (Figure 13b). With the knowledge of this new inverse slope ( $m$ ) and the x,y location of the midpoint, the y–intercept of this line ( $b$ ) can be computed. Thus, we now have the equation for the line

$$x = m y + b$$

The program then averages the two distances from the locations of the maximum and minimum to the origin and defines that value as the radius ( $R$ ) of the new circle which contains the maximum and minimum on its perimeter. The origin of this new circle lies at one of the

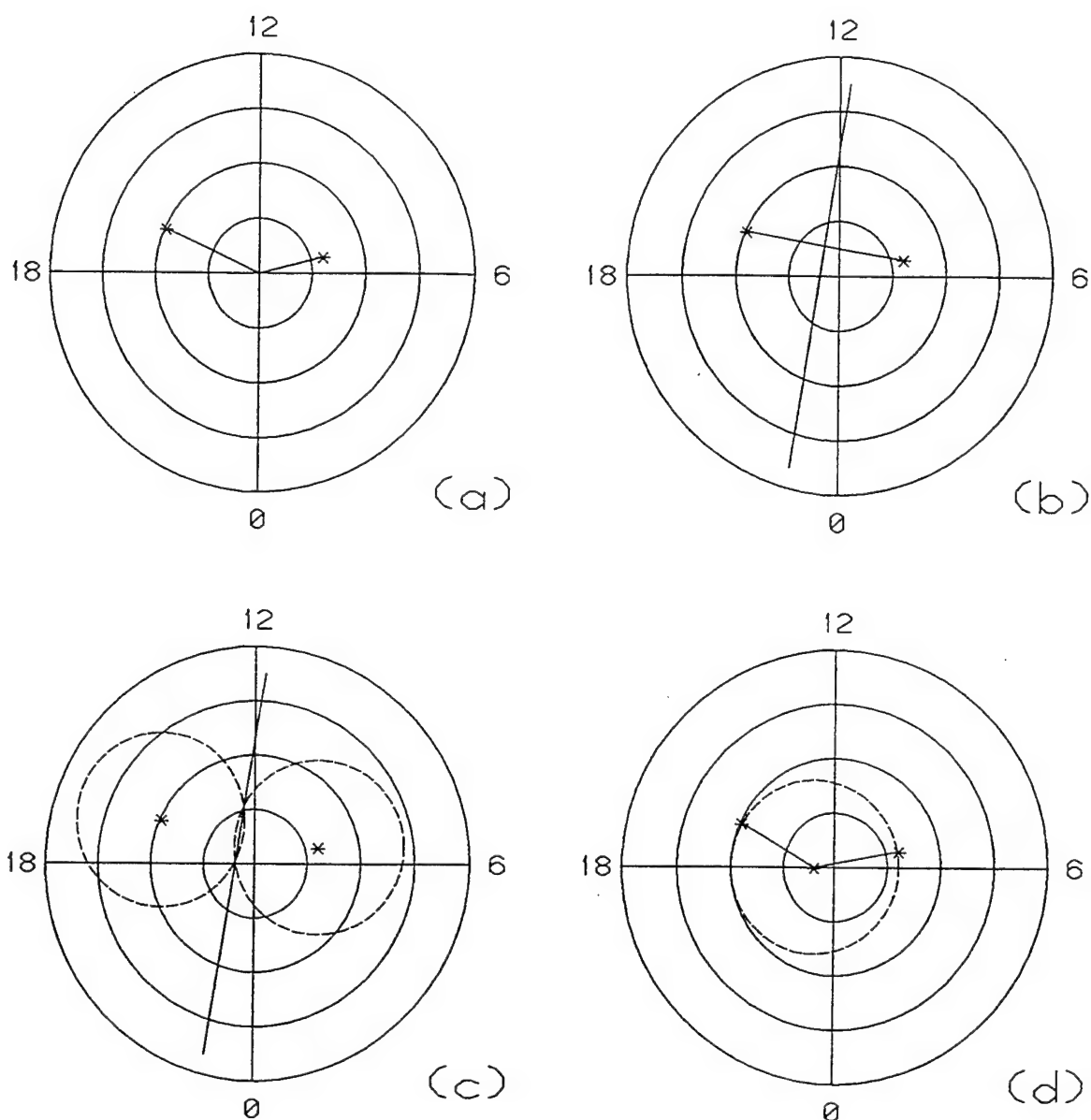


Figure 13. These figures illustrate the procedure for determining a circular convection reversal boundary which passes through the locations of the observed maximum and minimum. The locations of the maximum (dawnside) and minimum (duskside) are found relative to the origin and the two distances are calculated (a). Next the line between the maximum and minimum is determined, as is the line perpendicular to it and passing through the midpoint (b). Next, two circles of radius  $R$  (the average of the distance between the maximum and the origin and the distance between the minimum and the origin) are drawn centered on the locations of the maximum and minimum. There are two points where the circles and the perpendicular line intersect (c). The intersection point which is closest to the origin is selected as the origin of the new convection reversal boundary (a circle of radius  $R$  which contains the locations of the maximum and minimum on its perimeter) (d) and the location of the zero potential point relative to this new circle is used to match this pass to one of the three Heppner-Maynard patterns.

two intersecting points of the two circles of radius  $R$  centered on the maximum and minimum locations and the perpendicular line (Figure 13c). Thus, given the locations of the maximum  $(x_1, y_1)$  and the minimum  $(x_2, y_2)$ , we also have the equations

$$(x - x_1)^2 + (y - y_1)^2 = R^2$$

and

$$(x - x_2)^2 + (y - y_2)^2 = R^2$$

Thus, we have three equations and three unknowns, but only two of them are necessary to solve for the intersection points. Using the equation for the perpendicular line and the circle centered on the maximum, we can solve for the two intersection points. First, expand the equation for the circle.

$$(x^2 - 2x_1x + x_1^2) + (y^2 - 2y_1y + y_1^2) = R^2$$

Next, substitute the equation for the perpendicular line into this as the expression for  $y$  and  $y^2$  and bring the  $R^2$  term over to the left side, which gives

$$(x^2 - 2x_1x + x_1^2) + (m^2x^2 + 2mbx + b^2 - 2y_1mx - 2y_1b + y_1^2 - R^2) = 0$$

Rearranging the terms gives a quadratic equation

$$x^2 [1 + m^2] + x [2mb - 2x_1 - 2y_1m] + [x_1^2 + b^2 - 2y_1b + y_1^2 - R^2] = 0$$

The program calculates the values for each of the terms in the three sets of brackets, then uses them to solve for the two values of  $x$ . These are the  $x$  components of the two intersection points. The program finds the  $y$  components of the points by substituting the  $x$  values into the equation of the perpendicular line. The program then calculates the distances from each of these two points to the  $x$ - $y$  origin and chooses the closest one to be the new origin for the new convection reversal boundary circle (Figure 13d). After this, the code for this block continues on to locate the position of the zero point relative to this new circle and tests for the three Heppner–Maynard model just as it did in the earlier versions of DBASE4.

Testing of this new code showed that it corrected all of the wildly incorrect origins that

had appeared in the F9 processing. The testing also showed that, for the non-problem passes, the location of the new origins produced by the revised code exactly matched the locations of the new origins produced by the old code. Thus, the introduction of this change did not require the reprocessing of any previously processed data for the database.

## **7. Introduction to NADIA**

DBASE4 was designed to work under conditions where the datastream from the spacecraft was unbroken and the ionosphere was predominantly composed of ionized oxygen ( $O^+$ ). These were the conditions that existed in the late 1980s / early 1990s when DBASE4 was being developed. However, those conditions changed. As the spacecraft aged, the tape recorders broke down until, with F10, there was only a single operational tape recorder on board and thus there were large, regular data gaps which occurred when the recorder was played back to download the previous orbit's data. Also, the solar cycle entered its minimum phase, which resulted in the lowering of the fractional density of  $O^+$  ions at the DMSP orbital altitude. This drop in  $O^+$  ion density caused a degradation of the quality of data from the drift meter. These two problems required a revision of the DBASE4 code which was a major portion and deliverable of this contract. Initially this new code was referred to as DBASE5 in the proposal and in the progress reports. However, it was decided to rename this new version partially to denote the revision and partially to avoid the ongoing problem of possible confusion between this code and the commercial program "DBASE". Thus, this new version is now referred to as "NADIA" which stands for "Nominal / Anomalous (passes) Database for Ionospheric Analysis". The rest of this report will detail the new algorithms that have been integrated into NADIA.

## **NADIA part 1: Dealing with Data Gaps**

Originally, DBASE4 discarded any pass with a data gap of two minutes or longer in the polar region on the grounds that any gap that large would introduce unacceptable errors into the analysis and output. Under normal conditions this was a reasonable assumption, and since such passes occurred less than once per ten-days for the period 1988 through 1992, the loss of data from discarding these passes did not affect the overall quality of the output. But once F10 was reduced to a single tape recorder in 1993, the data gap during the downlink over Thule, Greenland during each orbit resulted in the removal of almost all the northern hemisphere passes. Although there was no way to recover the missing data from the downlink time, for the sake of the database and possible future space forecasting needs, it was necessary to revise the code in order to salvage as much of the data analysis from these passes as possible. Since the gap falls within the polar cap region under analysis, the calculation of the potential curve is affected and the results are degraded. The errors frequently mean that we cannot reliably determine where the zero potential point occurs in the pass and thus we cannot reliably match this pass to one of the Heppner–Maynard patterns. Figure 14 shows an example of a pass with a 2-minute gap in it. As can be seen from looking at this figure, while we cannot determine the Heppner–Maynard pattern for this pass, we can still calculate the locations and magnitudes of the potential maximum and minimum. Such information provides us with at least a lower bound on the polar cap potential drop, and that information can be fed into any of the operational models (either current or future versions) which require that information as an input. We define a new model number (IMODNUM) of 8 to indicate a pass which contains a data gap of more than two minutes within the polar cap and/or auroral region.

The technical description of the new algorithm for dealing with such passes is given as follows: In both DBASE4 and NADIA if there has been a data gap of more than 2 minutes

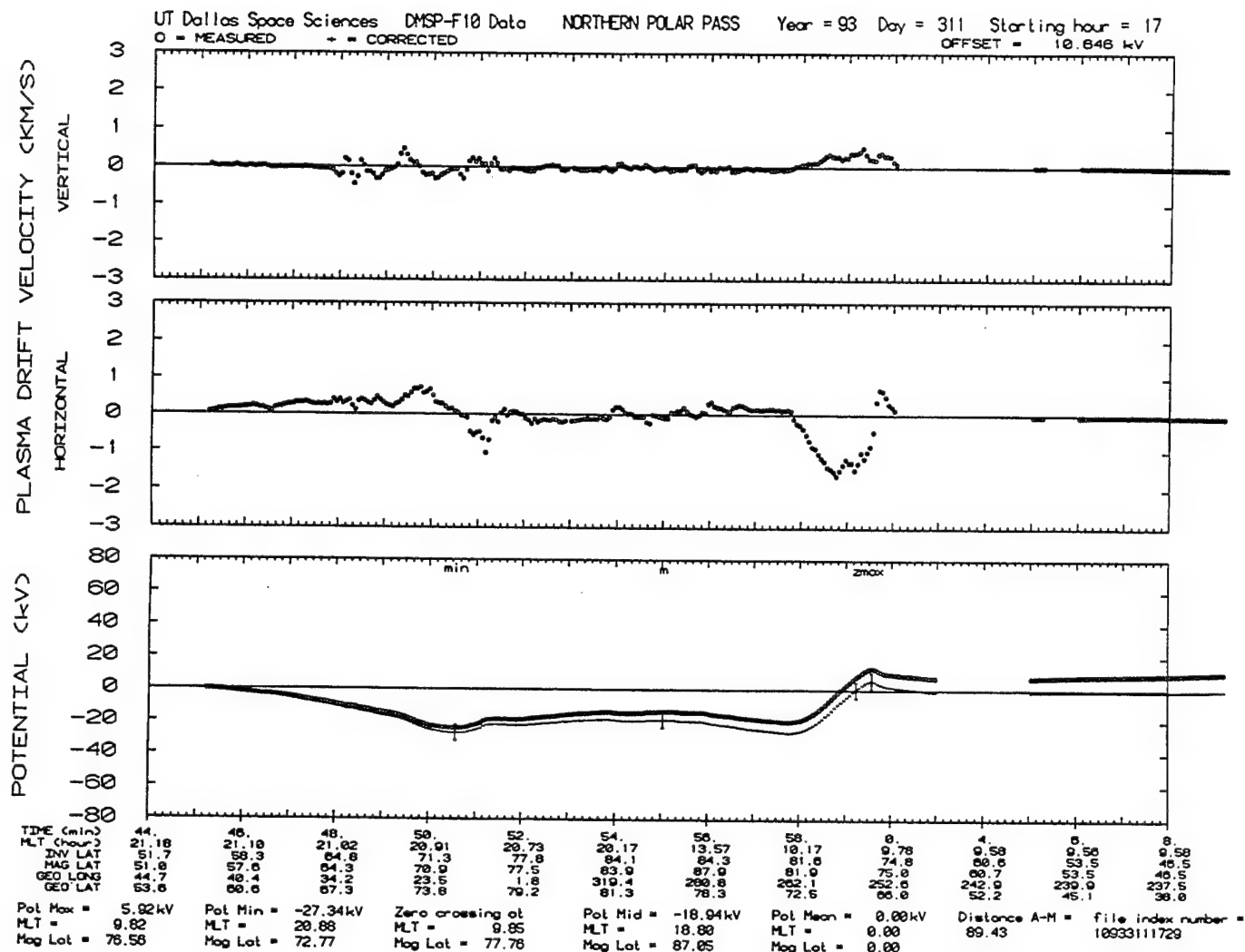


Figure 14. A typical northern pass with a two minute gap in the polar region. DBASE4 would discard such a pass immediately and return a null file. However, it is clear from the plot that most of the flow data are there, and that at least a lower bound on polar cap drop can be made from this pass.

detected while the data was being read by the subroutine IDMREAD, then the variable IMISS is set to 1. At the beginning of "Block 2A" there is now a check for the value of IMISS. If it is 0 (no gaps) then that pass continues on to the regular analysis routines. In DBASE4, if IMISS was 1 (a gap), then the pass was immediately discarded and a null file was generated. In NADIA the pass is not rejected immediately. Instead, it examines the entire dataset for gaps of two or more minutes. If it finds three gaps of that size or larger within the pass, then the pass is rejected on the grounds that there are too many missing data to make the salvage attempt worthwhile. However, if only one or two gaps are found, then this pass is sent on to the usual endpoint determination routine in "Block 2A". If one of the endpoints cannot be determined here, then this pass is discarded and a null dataset is returned (just as would happen with a normal pass without any gaps). If suitable endpoints are found for this pass with a data gap, then at the end of "Block 2A", there is one final check made on it. The time data for the pass (in array XUTIME) between the starting and stopping times in the polar region are examined to see if there are any gaps of two minutes or larger. If there is no gap within this period (i.e.—the data gap occurred outside of the region the program analyzes), then the program treats this pass like any other nominal pass. IMISS is reset to 0 and this pass is sent on to the normal analysis routine. However, if the algorithm detects a gap, then IMISS is left as 1 and IMODNUM is set to 8. This model number indicates that the pass has a data gap in it and so the results should be treated cautiously. The pass is then set on to the next block and a complete analysis is performed on it (just as if it were nominal pass without a data gap) until it reaches "Block 3F/G".

"Block 3F/G" is the part of the program where potential data are analyzed to determine if the pattern can be classified as one of the three Heppner–Maynard patterns, or a northward IMF case, or as one of the unusable cases. Since any zero crossing location resulting from the analysis of a pass with a data gap is suspect, then no attempt to fit this pass to

one of the Heppner–Maynard patterns is made. If the algorithm sees that this pass has already been classified as model number 8 (and that IMISS is also 1) at the beginning of “Block 3F/G”, it sets both the correction factors to 1.0 and sends this pass on to “Block 3H”. From there it continues until the data from this pass is written to the database, and then the program proceeds to the next pass for analysis.

The improvement in the analysis by using this new algorithm can be seen from the result obtained by comparing the outputs of DBASE4 and NADIA on the ten day period 1–10 November 1993 of F10 data. This period occurred during the time that F10 had only one functioning tape recorder and essentially all of the northern hemisphere passes were being thrown out as null passes.

Number of northern passes during in this dataset : 128

Using DBASE4 analysis

northern passes which were analyzable:	3 (2.3%)
northern passes discarded as null passes :	125 (97.7%)

Using NADIA analysis

northern passes which were analyzable:	83 (64.8%)
northern passes discarded as null passes :	45 (35.2%)

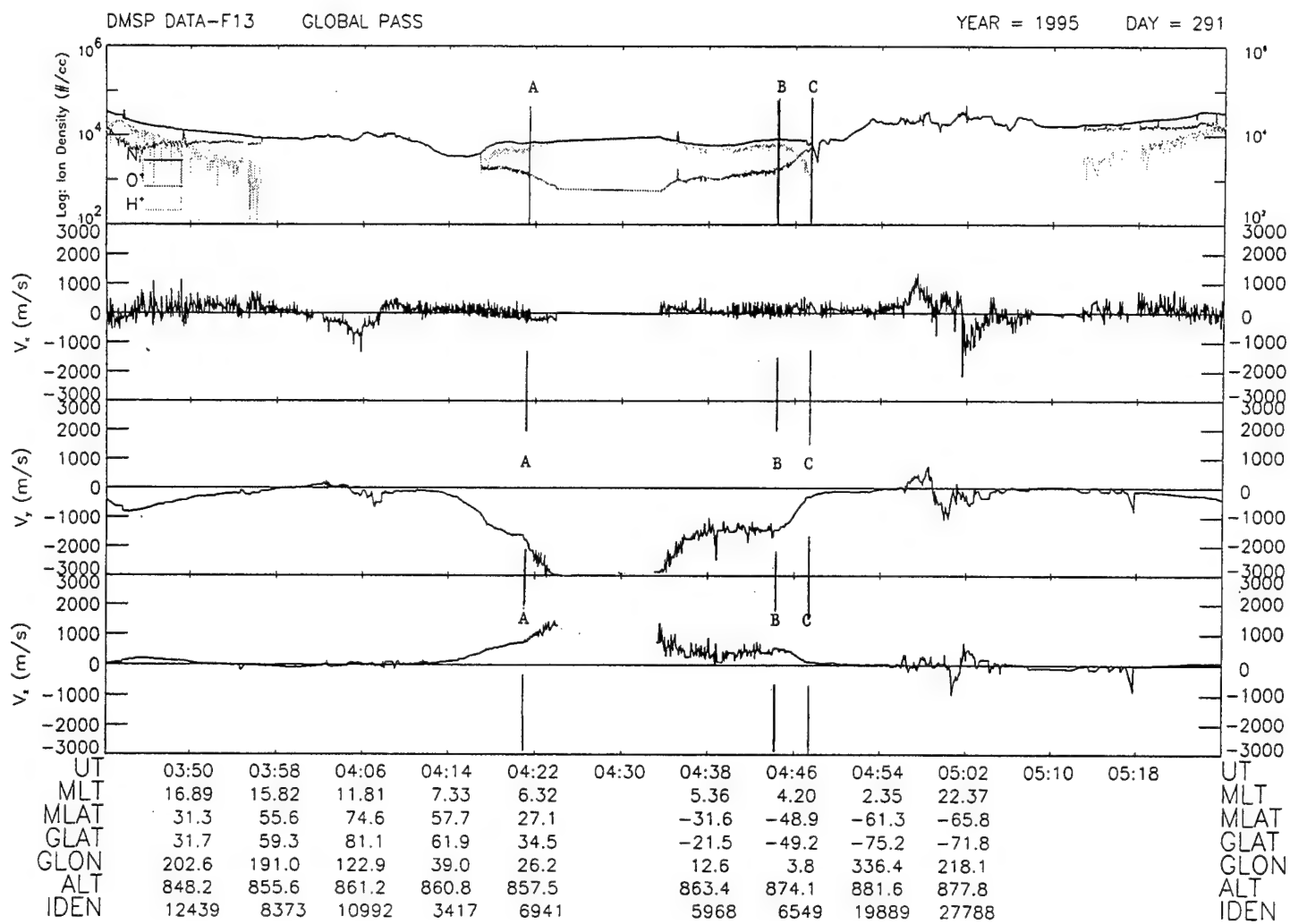
Of the 80 passes which could now be analyzed with NADIA, 62 of them were classified as model number 8. The other 18 were passes where the gap fell outside of the endpoints of the analysis, so the standard model analysis routine was performed. Two of them were categorized as model number 6 (unusable as either the maximum or minimum potential was zero), eight of them were categorized as model number 5 (skimmer passes), seven of them were categorized as model number 4 (zero occurred too far on the nightside for an unambiguous classification), and one was categorized as model 0 (northward IMF). None of the recovered passes from this dataset were categorized as one of the three Heppner–

Maynard patterns, but such an outcome is not impossible and may occur in other datasets. The remaining passes which could not be analyzed were rejected because the routine was unable to select suitable endpoints.

## **NADIA part 2: Dealing with Light Ion Plasmas and “Fuzzy” Endpoints**

One of the earliest problems encountered in the SSIES data was the phenomenon referred to as the “H+ fuzz” in the drift meter data (*Hairston and Heelis*, 1993). This was first observed in the earliest F8 data from summer 1987. The drift meter is specifically designed for operation in a predominantly O+ plasma environment. However, when the light ions (H+ and He+) become a significant fraction of the plasma (roughly more than 20%), the baselines of the cross track drifts shift away from zero. When the percentage density of O+ drops below about 20% of the total density, then the drift data begins to show a significant amount of scatter. Figure 15 shows one orbit of F13 data where both problems are apparent. The region between points A and B in the drift data occurred during a period when fraction of O+ ions was at 20% or less. The extreme scatter in the flow data is clearly seen here. (The gap in flow data occurred with the O+ density dropped so low that the drift meter “pegged” and went to the extreme values for both vectors. Here the horizontal flow went to an extreme negative value and the vertical flow went to an extreme positive value.) At point B the fractional O+ density went above 20% which eliminated the scatter, but both flows were still far from the zero baseline they should have been for these latitudes. Between points B and C the fraction of O+ increases until at C it passes the 80% mark and both flows return to the nominal zero or near zero values they should have at these latitudes.

The fraction of the ionosphere at 800 km which is composed of light ions is a function of the local time (dayside or nightside), the season, and the current status of the solar cycle.



WILLIAM B. HANSON CENTER FOR SPACE SCIENCES THE UNIVERSITY OF TEXAS AT DALLAS

Figure 15. A plot of an orbit of F13 showing the effects of low ion density and high relative light ion density on the drift meter output. See text for details.

F8 was launched in 1987 during the upswing towards solar maximum, so by 1988 the ionosphere was predominantly O+ at the DMSP orbital altitudes and no more problems with the "H+ fuzz" were observed in the data. However, by the beginning of 1994 the solar cycle was nearing its minimum, and as the percentage of light ions increased at the DMSP orbital altitudes, the problem with the "H+ fuzz" returned. During the daytime the problem is not too bad even during solar minimum. This is because ionization production keeps the relative O+ concentrations high during the daytime. However, once the sun sets the ionosphere begins to decay and the O+ concentration drops dramatically with respect to the lighter ions.

The specific behavior of the drift meter in the presence of light ions is not entirely understood, but we have developed a working scenario based on the observed data to explain this misleading behavior. So long as O+ dominates (i.e. – O+ is greater than 80%) the plasma entering the drift meter, the instrument works nominally, even down to low ( $10^3$  ion/cc) overall densities. Once the fraction of light ions increases above 20% of the overall density, then the flows begin to drift away from the zero baseline. It is suspected that the light ions (because of their light mass) are being deflected into the drift meter from some other part of the spacecraft. This is reasonable since the direction of the offset to the flow is always in the same direction regardless of the season or sun angle. Only a constant flow from some other part of the spacecraft could easily explain that fact. Thus, there are two components entering the drift meter: the O+ ions coming more or less straight into the detector and the light ions coming in at an extreme angle. Since the drift meter measures the ratio of the currents falling on the collectors, it averages the currents from the two components and outputs the results. So as the fraction of the light ions increases, the observed flow data move further away from zero baseline. If the O+ fraction drops to zero (as in the gap region in Figure 15 above) then there is nothing but the deflected light ions entering the

detector and the measured flow is "pegged" to one side. For regions where the fraction of O<sup>+</sup> is between 0 and 20% the instrument has trouble and the output begins to jump around. This is the "fuzzy" data region seen to the left of point B and the source of the name "H<sup>+</sup> fuzz". There is no way to determine absolutely whether this idea is correct other than possibly relocating the SSIES package on future DMSP spacecraft. However, this scenario is the best fit to the observed data from the drift meter seen under these conditions. In October 1995, the repellers in front of the drift meters on F12 and F13 were set to +2.0 volts (the repellers on all the satellites had been at 0 volts prior to this) to keep the light ions out but allowing the O<sup>+</sup> ions into the detector. Most of the problems have been solved by this and now when the O<sup>+</sup> density drops to zero, the signal from the drift meter goes to zero instead of "pegging" over at one extreme.

While the resetting of the repeller voltage has helped the problem for operational and future analysis, it is necessary to adapt the code to better handle passes with "fuzzy endpoints" in order to analyze most of the passes from the 1994–1995 time period. This adaptation was made in "Block 2A" and the algorithm is described below.

If one of the endpoint searches fails to determine an acceptable endpoint, the algorithm now considers whether this is a case of "H<sup>+</sup> fuzz". First it checks to see if the year is 1994 and earlier or 1995 and later. This division by date may not be appropriate for an operational version of the code. If the date is 1994 or earlier, then there is no point in conducting the search, so the program declares this to be a null pass and goes on. If the year is 1995 or later, then the program attempts to find a point where the standard deviations of the flows are less than 0.02 km/s ("H<sup>+</sup> fuzz" flow data characteristically have large standard deviations) but the acceptable magnitudes of the flows are larger than the limits used in the earlier search. The program does this by first determining the index numbers of the data at 40° and 35° magnetic latitude for this leg of the pass. It uses those indices to check

the values of both flow components at those magnetic latitudes. If all four values are outside the  $\pm 1.0$  km/s range, then this is declared to be an "H+ fuzz" case. (If any of the values are within  $\pm 1.0$  km/s, then the program declares this to be a null pass and goes on.) The program starts at the 40 degree magnetic latitude point and then begins working its way poleward looking for a point where the standard deviation of both the vertical and horizontal flow are less than 0.02 km/s (i.e.—a place that is not contaminated by "H+ fuzz"). There is a check in this search routine that stops it if the search reaches the highest magnetic latitude (index = ILIM2EQ) without finding a usable endpoint. In such a case, the program declares this to be a null pass and goes on. Once a point with acceptable standard deviations is found, the program then checks to see if the flow values for that point are both between  $\pm 0.5$  km/s. These are larger boundaries than were used in the regular search, but the "H+ fuzz" tends to result in larger flows at the endpoints. The value of 0.5 km/s was a compromise chosen as a result of testing part of the dataset. When limits of 0.4 km/s were used too many recoverable passes were discarded. Values as high as 0.7 km/s were also tested, but that caused endpoints too far away from the polar region to be selected. If the flows are too large, the search continues to the next point poleward.

Once a point with acceptable flow values and standard deviation values is found, the program then checks the next point poleward to see if it also satisfies this criteria. Once five acceptable points in a row are found, then the middle point is selected as the endpoint. The offset corrections for the endpoint (CHF1 and CVF1 for the starting point or CHF2 and CVF2 for the stopping point) are found by averaging the flow values for these five points. IMODNUM is set to 9 here to denote that this is an "H+ fuzz" recovered pass. The program then continues nominally to analyze the pass using this endpoint. However, once "Block 3F/G" (the model determination algorithm) is reached, then this pass is passed along without any further analysis. Since the endpoint determination is not fully certain for this pass,

its zero point location is suspect and thus it should not be considered for analysis as one of the Heppner–Maynard patterns. The data from this pass are output to the longfiles and shortfiles with a model number of 9.

This new algorithm was tested using data from both F12 and F13 (the spacecraft most affected by this problem) for both equinox and solstice conditions. The results are listed below.

**Table 2**

	total passes	total analyzable passes	model #9 passes
F12 21–25 September 1994			
DBASE4	125	17 (13.6%)	—
NADIA	125	60 (48%)	41 (32.8%)
F12 21–25 December 1994			
DBASE4	140	65 (46.4% all southern)	—
NADIA	140	101 (72.1% N and S)	35 (25%)
F12 21–25 March 1995			
DBASE4	140	40 (28.6% mostly south)	—
NADIA	140	100 (71.4% equal N & S)	58 (41.4% mostly north)
F12 21–25 June 1995			
DBASE4	140	51 (36.4% mostly north)	—
NADIA	140	99 (70.7% 2/3 north)	47 (33.6% equal N & S)

As can be seen from these numbers, NADIA improves the number of analyzable passes, but still cannot break the 75% level. Passes within the winter hemisphere are the most affected by the “H+ fuzz” problem and quite a number of them are beyond the possibility of being recovered. Even a “hands-on” analysis of these periods by the researcher would probably not produce results above 80%. Under solar minimum conditions and the present

SSIES design, it must simply be accepted that some fraction of the polar passes (usually in the winter hemisphere) produce data which cannot be sensibly analyzed.

F13 is in a more favorable orbit which minimizes its encounters with the "H+ fuzz" problem, so the results from it are better in general. However, this means that the improvement shown by using NADIA is not as great. The result of its tests are given below.

**Table 3**

	total passes	total analyzable passes	model #9 passes
F13 11–15 April 1995			
DBASE4	138	112 (81.2% 2/3 north)	—
NADIA	138	117 (84.8% 6/10 north)	5 (3.6% all south)
F13 22–26 June 1995			
DBASE4	141	91 (64.5% 3/4 north)	—
NADIA	141	115 (81.6% 2/3 north)	23 (16.3% all south)
F13 21–25 September 1995			
DBASE4	127	110 (86.6% ~equal N & S)	—
NADIA	127	116 (91.3% ~equal N & S)	5 (3.9% all south)

Careful examination of the results here shows that there are a few extra new passes which appear in the NADIA results. These are all model 4 through 8 results which were declared null passes by DBASE4.

Thus, there are currently 10 possible model numbers that can be output by NADIA to a shortfile, so the full list of models and their interpretations is now:

- 0 – northward IMF ( $\Delta \text{PSI} < 40 \text{ kV}$ , highest magnetic latitude point  $> 75$  degrees) or else a null pass when all other elements in the shortfile are also zero
- 1 – HM model BC
- 2 – HM model A
- 3 – HM model DE
- 4 – unusable (zero occurred in far nightside or else pattern is too distorted to classify unambiguously)
- 5 – skimmer (unusable— $\Delta \text{PSI} < 10 \text{ kV}$ )
- 6 – unusable (either observed maximum or minimum potential was zero)
- 7 – unusable (one of the corrections greater than 10 or negative, pattern likely too distorted to classify unambiguously)
- 8 – data gap of two minutes or longer occurred within the polar region analyzed,  $\Delta \text{PSI}$  can be used to give a lower bound on the true polar cap potential drop
- 9 – one or more endpoint was missing because of the light ion fuzz in the drift meter data, the analysis is cut off at the beginning of the fuzzy region,  $\Delta \text{PSI}$  can be used to give a lower bound on the true polar cap potential drop

## 8. Conclusion

The work during this period has improved the performance and reliability of the DBASE4 / NADIA code and algorithms being used for the polar cap potential drop measurement and the convection pattern analysis. However, this work has also pointed up the limits of current operational reliance on the Heppner–Maynard models of the ionosphere. Just as meteorological forecast models require more than three possible weather maps to describe the current conditions over North America, truly accurate space weather forecast models will require a larger number and more sophisticated set of models for the polar ionosphere. Such models should be adaptable to model inputs and will need to be based not only on the current IMF conditions, but also on the recent history of the IMF and the ionosphere, as well as season and phase of the solar cycle.

To date, investigators have been limited to generalized models such as the Heppner–Maynard models simply because the datasets of ionospheric flow data on which such models were based were so limited. However, the DMSP SSIES database currently holds *more than 20 satellite-years* of near continuous data covering almost an entire solar cycle. Such a tremendous wealth of data means that it is now possible to begin building such sophisti-

cated and quantitative models of the ionospheric convection. It is anticipated that such work will be the logical follow-up to this contract.

## **9. Recommendation for Future Work**

It is clear from the previous report that, while a single polar pass by a DMSP spacecraft can give an accurate output of the potential observed along that particular pass, trying to extrapolate the true total cross-cap potential drop (one of the key inputs to the MSM and MSFM) from those data has had only limited success. The main limitation comes from trying to force all the southward IMF passes to conform to one of the three Heppner-Maynard patterns. This is somewhat akin to trying to forecast the terrestrial weather over the US while being limited to only three generic weather maps. It is obvious from examining the DMSP database that there are a wide variety of potential distribution patterns which can occur in the polar regions under a wide range of conditions. The large existing DMSP database would provide an excellent resource for developing a series of potential distribution models which could be scaled to fit a given pass in order to extrapolate the true cross-cap potential drop. Beside being more flexible and accurate, such models would be used for northward IMF cases and would, for the first time, provide error bars to their estimates of the true maximum and minimum potentials. Such an analysis using these advanced models would fall naturally within the NADIA code.

After several years of work on the algorithms which choose the endpoints, it is apparent that we are reaching the limit of the effectiveness of the selection procedures based on simple analysis of the flow data. If all the passes were nominal, where the flows were steady and close to zero outside of the auroral region, then a straightforward algorithm would be all that was needed. However, experience shows that in the DMSP data stream there are a wide variety of different flows seen outside of the auroral region, some caused by "H+

fuzz", some caused by drifts in the flow's baseline, etc. No single algorithm or group of algorithms has been able to work on all possible cases encountered by the spacecraft. The choice of appropriate endpoints, a task which seems so obvious to even an untrained observer looking at the flow data, has proven frustratingly difficult to achieve using a relatively small algorithm. This problem appears to be an ideal candidate for the development of a neural network pattern recognition program which could provide better choices of the endpoints for the pass. If further work on improving the endpoint selection is required, neural networks should be explored as a possible solution.

It should also be noted that there will be some differences in the telemetry formatting between the current SSIES-2 and the forthcoming SSIES-3 (beginning with Block 5 on F16). While the drift meter data will still be taken at the same resolution (6 times per second for each component) and the analysis part of the program will be unchanged, there will have to be some work done on the "front end" of the program which reads the telemetry and prepares it for analysis. There will at least need to be some work done to verify that the analysis routines are working properly with the new SSIES-3 telemetry. There is also a lower resolution mode for the drift meter where it samples each flow component only once per second. This mode was designed for use in regions of low ion density where the current SSIES-2 design has trouble taking measurements. If this mode is employed, then some more adjustments to the code will have to be made to the part which converts the telemetry to flow data and averages it into four-second bins. Once the flow data are in the four-second bins, none of the analysis code past that will need to be changed.

## Appendix: Scientific Papers Published and Professional Talks Given During this Contract

### Papers:

Hairston, Marc R., Roderick A. Heelis, and Frederick J. Rich, Visualization of the electrostatic potential distribution in both polar ionospheres using multiple satellites, in *Visualization Techniques in Space and Atmospheric Sciences*, edited by E. P. Szuszczewicz and J. H. Bredekamp, National Aeronautics and Space Administration, SP-519, 1995.

Cumnock, J. A., R. A. Heelis, M. R. Hairston, and P. T. Newell, High-latitude ionospheric convection patterns during steady northward interplanetary fields, *J. Geophys. Res.*, 100, p. 14537, 1995.

Hairston, Marc R. and Roderick A. Heelis, Response time of the polar ionosphere to changes in the North-South direction of the IMF, *Geophys. Res. Letts.*, 22, p. 631, 1995.

Rich, F. J. and M. R. Hairston, Large-scale convection patterns observed by DMSP, *J. Geophys. Res.*, 99, p. 3827, 1994.

Knipp, D. J., B. A. Emery, A. D. Richmond, and M. R. Hairston, Mapping ionospheric convection responses to IMF  $B_y$  negative and  $B_z$  positive conditions, *J. Atmos. Terr. Phys.*, 56, p. 223, 1994.

Knipp, D. J., B. A. Emery, A. D. Richmond, N. U. Crooker, M. R. Hairston, J. A. Cumnock, *et al.*, Ionospheric convection response to slow, strong variations in a northward interplanetary field: A case study for 14 January 1988, *J. Geophys. Res.*, 98, p. 19273, 1993.

### Professional talks given:

Hairston, Marc R., Roderick A. Heelis, and Frederick J. Rich, *Polar ionospheric pattern models based on the location of the high latitude zero potential line using DMSP data*, Fall 1995 AGU Meeting, SA52A-4

Hairston, Marc R., Roderick A. Heelis, and Frederick J. Rich, *Analysis of cross polar cap potential drop and ionospheric convection patterns using DMSP data for Space Weather Forecasting*, Summer 1995 GEM meeting, Snowmass Colorado

Hairston, Marc R., Roderick A. Heelis, and Frederick J. Rich, *Analysis of cross polar cap potential drop and ionospheric convection patterns using DMSP data for Space Weather Forecasting*, Spring 1995 AGU Meeting, SA21A-2

- Hairston, Marc R. and Roderick A. Heelis, *Plasma and field characteristics of simultaneous theta aurora in both polar ionospheres using DE and DMSP data*, Fall 1994 AGU Meeting, SM42A-11
- Cumnock, J. A., R. A. Heelis, and M. R. Hairston, *The high-latitude ionospheric convection pattern during steady northward IMF*, Fall 1993 AGU Meeting, SA32A-2
- Hairston, Marc R., Roderick A. Heelis, and Frederick J. Rich, *Response time of the ionospheric convection pattern to changes in the IMF*, Fall 1993 AGU Meeting, SA32A-7
- Cumnock, J. A., R. A. Heelis, and M. R. Hairston, *Sunward convection observed by DMSP F8 at high latitudes*, Spring 1993 AGU Meeting, SM31B-8
- Hairston, Marc R., Roderick A. Heelis, and Frederick J. Rich, *Visualization of the electrostatic potential distribution in both polar ionospheres using multiple satellites*, Spring 1993 AGU Meeting, SM32A-6

## References

- Hairston, M. R., and R. A. Heelis, High-latitude electric field studies using DMSP data, PL-TR-93-2036, Phillips Lab., Directorate of Geophys., AF Materiel Command, Hanscom AFB, MA, 18 February 1993, ADA265032.
- Hairston, Marc R. and Roderick A. Heelis, Response time of the polar ionosphere to changes in the North-South direction of the IMF, *Geophys. Res. Letts.*, 22, p. 631, 1995.
- Heelis, R. A., and M. R. Hairston, Studies of ionospheric dynamics utilizing data from DMSP, GL-TR-90-0047(I), Air Force Geophys. Lab. Hanscom AFB, MA, April 1990, ADA223370.
- Heppner, J. P., and N. C. Maynard, Empirical high-latitude electric field models, *J. Geophys. Res.*, 92, p. 4467, 1987.
- Rich, F. J. and M. R. Hairston, Large-scale convection patterns observed by DMSP, *J. Geophys. Res.*, 99, p. 3827, 1994.